

Theory of enhanced-by-coincidence neural information transmission

Miguel Ibáñez-Berganza*

*IMT School for Advanced Studies Lucca, Piazza San Francesco 19, 50100, Lucca, Italy and
INdAM-GNAMPa Istituto Nazionale di Alta Matematica ‘Francesco Severi’, P.le Aldo Moro 5, 00185 Rome, Italy*

Giulio Bondanelli

*Neural Computation Laboratory, Istituto Italiano di Tecnologia, Genoa, Italy and
Institute for Neural Information Processing, Center for Molecular Neurobiology,
University Medical Center Hamburg-Eppendorf, 20251, Hamburg, Germany*

Stefano Panzeri

*Institute for Neural Information Processing, Center for Molecular Neurobiology,
University Medical Center Hamburg-Eppendorf, 20251, Hamburg, Germany*

(Dated: February 17, 2025)

The activity of neurons within brain circuits has been ubiquitously reported to be correlated. The impact of these correlations on brain function has been extensively investigated. Correlations can in principle increase or decrease the information that neural populations carry about sensory stimuli, but experiments in cortical areas have mostly reported information-limiting correlations, which decrease the information encoded in the population. However, a second stream of evidence suggests that temporal correlations between the spiking activity of different neurons may increase the impact of neural activity downstream, implying that temporal correlations affect both the encoding of information and its downstream readout. The principle of how encoding and readout combine are still unclear. Here, we consider a model of transmission of stimulus information encoded in pre-synaptic input spike trains with information-limiting time-correlations to the output firing of a post-synaptic biologically-plausible leaky integrate and fire (LIF) readout neuron. We derive an analytical solution of the model in the diffusion approximation, in which the encoding spiking activity is treated as a continuous-time stochastic variable. An ansatz based on a separation of timescales allows us compute the stimulus information transmitted to the readout over a broad range of parameters. Our analytical results reveal that, for sufficiently low input firing rates, large enough difference in input stimulus-specific activity, and moderately large input temporal correlations, the stimulus discriminability of the firing of the LIF readout neuron can be enhanced by the presence of input time correlations, despite they decrease the stimulus information encoded in its inputs.

I. INTRODUCTION

Since the first extensive simultaneous recordings of the activity of multiple neurons in the brain *in vivo* were performed decades ago [1–6], neuroscientists have consistently observed that the times at which different neurons fire are correlated. That is, the timing at which a neuron fires does not depend only on externally-measurable correlates as the sensory stimulus or the animal’s decision, but also on the timing of firing of other neurons. When considering the encoding of sensory stimuli, correlations are usually measured as so called *noise correlations*, defined as correlations between the timing of spikes of different neurons at a fixed value of the sensory stimulus [7, 8].

Previous work has shown that noise correlations between the spike timing of different neurons is related to their anatomical connectivity [9]. However, despite being ubiquitously reported across brain activity recordings *in vivo*, their possible contribution to brain function remains intensively debated. Theoretical work has shown that temporally correlated inputs can profoundly affect the dynamics of spiking neuron models [10–22]. It has been proposed that one function of such correlations is to shape the amount of information that can be encoded in a neural population [7, 8, 22–25]. In particular, these studies have shown that noise correlations can have both an information-enhancing effect or an information-limiting effect on the information carried by a population of neurons [7, 25–29]. However, the majority of empirical studies analyzing neural recordings have reported information-limiting correlations [29], defined here as correlations that decrease the amount of information in a neuronal population [26, 30–32]. This has led to the widespread view that noise correlations eventually limit the ability of an organism to discriminate sensory stimuli, thus impairing perceptual discrimination and decision-making [26, 29, 31, 33].

* miguel.ibanezberganza@imtlucca.it

However, recent experimental findings have challenged this notion, reporting that noise correlations are stronger during correct than during incorrect perceptual judgments [32, 34–38], suggesting that noise correlations benefit perceptual abilities. This has been reported even in experiments in which noise correlations are information-limiting, ruling out that this effect may be due to enhanced encoded information. While some of these results can be understood also neglecting neural dynamics and considering only time-averaged responses [39], they have a natural explanation considering the time-dependent nature of neural correlations and neural information encoding and transmission. Temporally-correlated presynaptic activity can elicit stronger responses in postsynaptic neurons with short integration time constants via the non-linear mechanism of coincidence detection [24, 40]. Under such conditions, noise correlations can amplify responses in downstream neural populations and thus increase the amount of sensory information that is transmitted downstream, despite reducing the *encoded* input information. In particular, stronger information-limiting noise correlations may make different neurons more redundant, which enhances the consistency of stimulus-encoding neural responses across time and neurons. A downstream neuron with short integration time constants may exploit the enhanced consistency in its input to outweigh the information-limiting effects of noise correlations, ultimately increasing the stimulus information that is read out downstream [32, 41].

Understanding the feasibility of such an enhanced-by-coincidence information transmission between pre- and post-synaptic activity requires models of neurons as physical systems that integrate both stimulus encoding and readout mechanisms. A biologically plausible Neural Encoding and Readout Model (NERM) was proposed by Valente et al. (2021) [32]. This model consists of a population of pre-synaptic neurons encoding a binary stimulus, which subsequently drives a single post-synaptic readout neuron. The encoding neurons generate spike trains with a certain strength and time scales of correlation across neurons. These correlations are designed to be information-limiting, that is to decrease the information encoded in the input when the strength of correlation increases. The readout neuron is modeled as a leaky integrate-and-fire (LIF) neuron and integrates afferent currents as a weighted sum of spike trains with a given membrane integration time constant. Numerical solutions of this model reveal that the stimulus discriminability of the readout neuron (as quantified by the signal-to-noise ratio between the difference in stimulus-specific mean firing rates and its variance, SNR) can be, seemingly paradoxically, enhanced by stronger information-limiting correlations for sufficiently short readout time constants and sufficiently low input firing rate. In these conditions correlations amplify the stimulus information transmitted to the readout even when decreasing input information.

This previous study left open important questions about the conditions needed for noise correlations to overcome their information-limiting impact at the readout stage. The study of the model was limited to only $N = 2$ input encoding neurons, while information transmission in the brain involves larger neural populations. Moreover, this previous study has not provided an analytical understanding of the interplay between encoding and readout of information in neural populations. To overcome these issues and allow an understanding of these neural operations as a statistical physical system, we develop an analytical framework to characterize the SNR enhancement effect beyond numerical simulations. This framework allows to study encoding in a population with an arbitrary number N of pre-synaptic input neurons with time-dependent correlations, and study how this information is transmitted to a readout LIF neuron. The ability to obtain solutions for arbitrary input population sizes allows us to study the interplay between the spatial dimension of population size (including the large N limit) and the time scales of input correlations and of readout integration. Our approach employs a diffusion approximation, where the readout neuron membrane potential obeys a second-order stochastic differential equation. In this framework, the inter-spike interval (ISI) of the readout neuron corresponds to the first passage time of an *inertial* stochastic process. We derive analytical expressions for the mean and variance of the readout neuron firing rate, and its temporal correlation structure. Treating this problem within the theory of stochastic processes involves analyzing first-passage times of non-Markovian random walks, which typically requires solving coupled Fokker-Planck equations. By introducing a novel analytical approach—the *quenched-noise approximation*—we provide tractable expressions for the firing rate mean and variance under the assumption that the noise correlations timescale τ_c is much larger than the membrane time constant of the readout neuron τ_m . The quenched-noise approximation exploits classical expressions for the mean rate of the LIF neuron with white noise input [42]. Our results extend previous expressions for the mean rate of LIF neurons with colored noise input with $\tau_m \ll \tau_c$ [17], which were recovered in the limit of weak correlation strength. Moreover, we are able to study analytically the opposite limit $\tau_c \ll \tau_m$ using a Poisson approximation. These results provide the necessary conditions for noise correlations to enhance the readout SNR. Notably, our analysis demonstrates that SNR enhancement can occur for a wide range of noise correlation timescales τ_c , regardless of whether they exceed or fall below the membrane time constant τ_m .

The article is structured as follows. We first define the NERM (Sec. II). We then (Sec. III) investigate how a readout LIF neuron with or without time-correlated inputs discriminates between binary stimuli s by computing the SNR of its firing activity. In Sec. III A, we approximate analytically the SNR using the mean and variance of the firing rate of a LIF neuron with input current satisfying a scalar Ornstein-Uhlenbeck equation, within the quenched-noise approximation in the $\tau_c \gg \tau_m$ regime (Secs. III B, III D). In Sec. III C, we explain intuitively why and when noise

correlations enhance downstream stimulus information transmission under the quenched-noise approximation. In Sec. IV we describe analytically how noise correlations influence the readout SNR. We finally draw conclusions in Sec. V.

II. DEFINITION OF THE NEURAL ENCODING-READOUT MODEL (NERM)

To study the impact of noise correlations at the encoding (input, pre-synaptic) stage on a post-synaptic readout neuron, we consider the biophysical Neural Encoding-Readout Model (NERM) defined in [32]. The NERM consists of a population of N neurons encoding a binary stimulus $s = \pm 1$, and a single readout neuron that integrates the neural activity of the encoding population (see Figs. 1,2,3).

The pre-synaptic encoding neurons are modeled as N inhomogeneous Poisson processes with stochastic coupled firing rates. For stimulus s , the firing rates of the encoding population $\mathbf{x}^{(s)}(t)$ satisfy the multivariate Ornstein-Uhlenbeck process given by:

$$\tau_c \dot{\mathbf{x}}(t) = (\boldsymbol{\mu}^{(s)} - \mathbf{x}(t)) + \sqrt{2\tau_c C} \cdot \boldsymbol{\eta}(t), \quad (1)$$

where $\boldsymbol{\eta}(t)$ is the vector of across-time and across-neuron uncorrelated white noises, $\boldsymbol{\mu}^{(s)}$ the stimulus-specific mean activity (or tuning curve), C the stationary across-neuron covariance matrix and τ_c the correlation timescale (see Table II in Appendix A). Thus, the resulting firing rates are correlated across neurons with covariance C and across time with timescale τ_c , with first and second moments given by $\langle x_j^{(s)}(t) \rangle_{\boldsymbol{\eta}} = \mu_j^{(s)}$ and $\langle (x_i^{(s)}(t') - \mu_i^{(s)})(x_j^{(s)}(t' + t) - \mu_j^{(s)}) \rangle_{\boldsymbol{\eta}} = C_{ij} e^{-|t|/\tau_c}$, where the expectation values $\langle \cdot \rangle_{\boldsymbol{\eta}}$ are computed across white noise realizations [43, 44]. We define the matrix of *noise correlations*, \bar{C} , as $\bar{C}_{ij} := C_{ij}/(v_{V_i} v_{V_j})^{1/2}$, where $v_{V_j} := C_{jj}$ is the *stationary variance* of the j -th neuron rate. The corresponding *spike count variance* is $\sigma_{V_j}^2 = 2\tau_c v_{V_j}^2$ (see Appendix A for a discussion about the stationary vs spike count variance terminology). The noise correlation matrix is defined to exhibit equal off-diagonal elements, i.e. $\bar{C}_{ij} = \alpha_V$ for $i \neq j$, where the fraction of shared noise $\alpha_V \in [0, 1]$ modulates the shared over private noise ratio, so that the limiting cases $\alpha_V = 0, 1$ represent completely uncorrelated and correlated encoding firing rates respectively. To ensure that the noise correlations are information-limiting, we set the noise amplitude σ_{V_i} to be proportional to the difference of tuning curves $\sigma_{V_i} = \nu_V \Delta\mu_i$, where $\Delta\mu_i := \mu_i^{(+)} - \mu_i^{(-)} > 0$ with $\nu_V > 0$ (see [32] and equation (8) below).

Given stimulus-specific firing rates $\mathbf{x}^{(s)}(t)$, the spike train of the i -th encoding neuron $(t_{m_i}^{(i)})_{m_i}$ in the time interval $[0, T_c]$ is sampled from an inhomogeneous Poisson process with underlying firing rate $x_i^{(s)}(t)$ (see Fig. 2 and Appendix B), so that the encoding spike trains are generated through a doubly stochastic process. Given the encoding spike trains, the response of the readout neuron is deterministic.

The postsynaptic readout neuron is modeled as a leaky integrate-and-fire (LIF) neuron [42, 45] that receives the spike trains of the encoding neurons as inputs, weighted by the vector synaptic strengths \mathbf{w} . The dynamics of the readout neuron membrane potential $V(t)$ is given by:

$$\dot{V}(t) = -V(t)/\tau_m + I(t) \quad (2)$$

$$I(t) = \sum_{i=1}^N w_i \sum_{m_i > 0} \delta(t - t_{m_i}^{(i)}), \quad (3)$$

with firing threshold $\Omega = 1$, and where $(t_{m_i}^{(i)})_{m_i}$ is the spike train of the i -th encoding neuron. Note that, following previous work [17, 32, 46], the above equation assumes that the synapses are instantaneous (without a rise time or a synaptic decay time constant, which would have been more realistic). This implies that all the temporal post-synaptic integration properties of the readout neuron depend on its membrane time constant τ_m . The readout neuron spiking times will be referred to as $\vec{t} = (t_1, \dots, t_{n_R}(T_c))$, where $n_R(T_c)$ is the number of readout spikes in the time window of length T_c in a single realization of the encoding spike trains.

Examples of the dynamics of the input spike trains at the encoding stage and of the membrane and spiking dynamics of the readout neuron are given in Fig 2 for the case of correlated inputs ($\alpha_V = 0.9$) and in Fig. 3 for the case when correlations in the input are set to zero ($\alpha_V = 0$). Note that the input activity of the model with $\alpha_V = 0.9$ exhibits clearly visible covariations over the 100 ms time-scale set by the Ornstein-Uhlenbeck process (Fig 2) compared to the $\alpha_V = 0$ case. The output of the readout neuron has higher firing and higher rate separation (and thus higher stimulus-discriminative signal) between the rates elicited by the two stimuli, because correlations in inputs increase the frequency of events with near-coincident firing in the input compared to the uncorrelated-input case (Fig. 3).

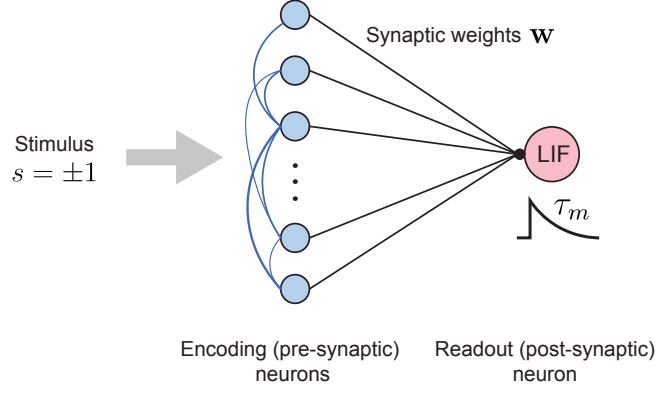


FIG. 1. *Illustration of the Neural Encoding-Readout Model (NERM).* A binary stimulus s is encoded in the time-dependent activity of a population of N encoding pre-synaptic neurons, whose firing rates $\mathbf{x}^{(s)}(t)$ are the solution of an Ornstein-Uhlenbeck process, that depends on s through the average firing rate vector $\boldsymbol{\mu}^{(s)}$. Given the firing rate vector $\mathbf{x}^{(s)}(t)$, the encoding neural activity consists of a set of N spike trains in a time window $[0, T_c]$, with spiking times drawn from a multivariate inhomogeneous Poisson process with underlying firing rate $\mathbf{x}^{(s)}(t)$. The encoding spike trains, weighted by the vector of synaptic weights \mathbf{w} , constitute the afferent input current of the readout LIF neuron. The stimulus-specific response of the readout is characterized in terms of the mean and variance ($r_R^{(s)}, v_R^{(s)}$) of the readout neuron firing rate.

However, input correlations also increase the variability, or noise, of the readout neuron output rate, which makes it difficult to understand whether input correlations increase or decrease the output information without a careful quantification of both signal and noise as function of the parameters of the model.

To examine how well the stimulus can be discriminated from the readout spike trains, we consider, as in [32], the (square root of the) *Signal-to-Noise Ratio* (SNR), defined as:

$$\text{SNR} = \frac{r_R^{(+)} - r_R^{(-)}}{[(v_R^{(+)} + v_R^{(-)})/2]^{1/2}}, \quad (4)$$

where $r_R^{(s)}$ and $v_R^{(s)}$ are the stimulus-specific average and variance of the readout rate $n_R(T_c)/T_c$ over the distribution of readout spike trains \vec{t} , i.e. $\text{prob}(\vec{t}|s)$ (see Table II). In our numerical analyses, we focus on the SNR *in the unit time interval* $\text{SNR} \times T_c^{-1/2}$, since the rate variance decreases as T_c^{-1} (Eq. (11)) and the SNR increases as $T_c^{1/2}$.

III. ANALYTICAL RESULTS ON THE READOUT LIF MODEL WITH COLORED-NOISE INPUT CURRENT

A. The diffusion approximation for the encoding signal

To build an interpretable theory of the NERM, we will first adopt the *diffusion approximation* for the readout neuron afferent current $I(t)$ in Eq. (3) [17, 42, 45]. This approximation is based on the fact that for high enough input spike count $x_i(t)\delta$ in a time window δ the Poisson statistics of the count $n_i(t+\delta) - n_i(t)$ approaches a normal distribution with mean and variance equal to $x_i(t)\delta$. In the diffusion approximation, the input current $I(t)$ and the readout neuron membrane potential $V(t)$ in Eq. (2) satisfy (see Appendix B and [17]):

$$\dot{V}(t) = -V(t)/\tau_m + I(t) \quad (5a)$$

$$I(t) = \mu_I + \sigma_I \eta(t) + \sigma_c \xi(t) \quad (5b)$$

$$\dot{\xi}(t) = -\xi(t)/\tau_c + \frac{1}{\tau_c} \eta'(t) \quad (5c)$$

where η, η' are two different white noises, and $\xi(t)$ is an Ornstein-Uhlenbeck process with timescale τ_c . In the diffusion approximation the density of encoding spikes $I(t)$ in Eq. (3) can be treated as a scalar stochastic current with *mean* μ_I , *white noise amplitude* σ_I , and *colored noise amplitude* σ_c given by:

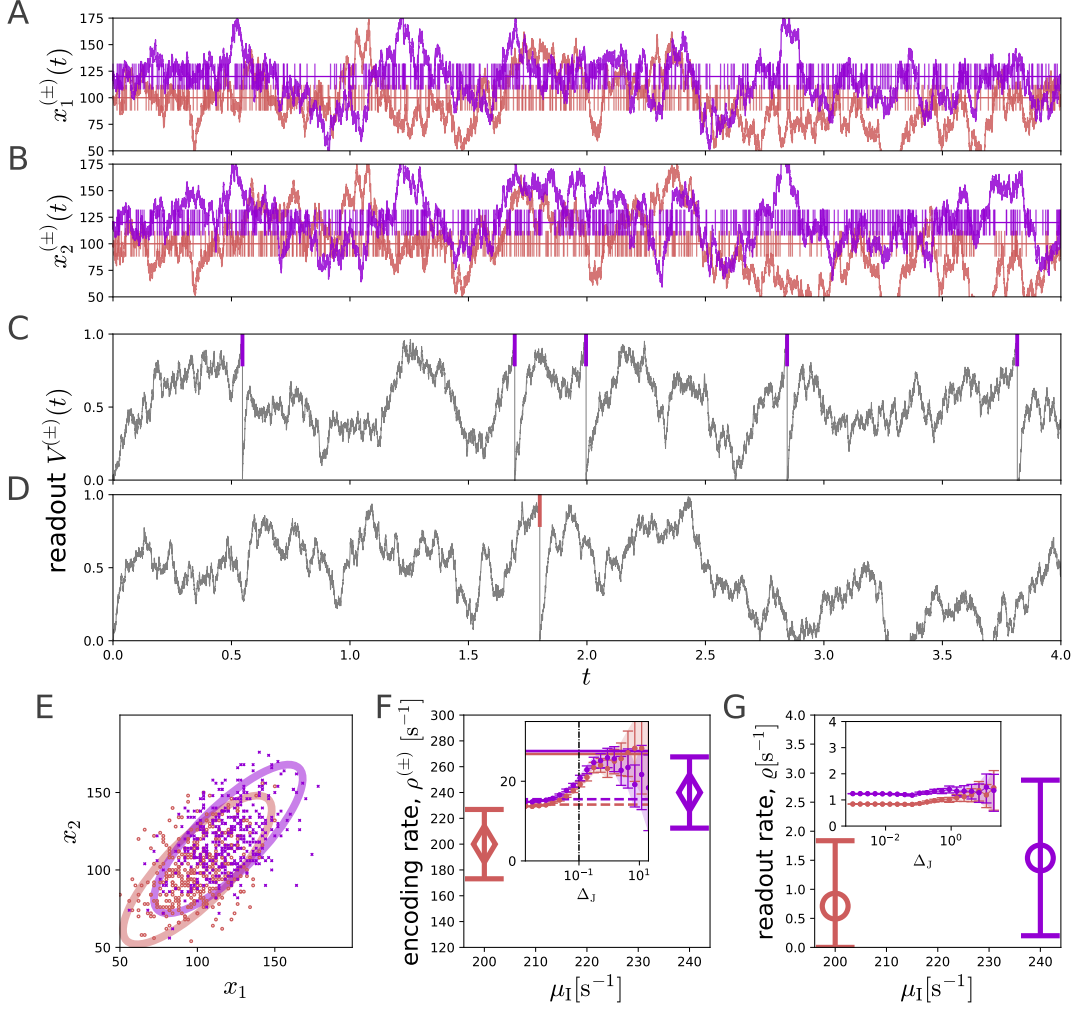


FIG. 2. *Neural activity in the Neural Encoding and Readout Model with $N = 2$ encoding neurons and a strong degree of noise correlation alignment $\alpha_V = 0.9$.* (A-B) Encoding firing rates $x_{1,2}^{(s)}(t)$ (continuous curves in A,B) and spike trains sampled from an inhomogeneous Poisson process with rate $x_{1,2}^{(s)}(t)$ are shown in a time window $[0, T = 4]$ s for stimuli $s = \pm 1$ (orange and violet, respectively). (C-D) LIF membrane potential $V(t)$ (grey lines) and spike times (ticks) for $s = +, -$ (respectively panels C and D). (E) Encoding spike density $(n_1(\Delta), n_2(\Delta))$ in different time windows of size $\Delta = 0.5$ (for a simulation that lasts up to $T_c = 100$). The ellipse axes are oriented along the eigenvectors of \bar{C} , and their lengths are proportional to the corresponding eigenvalue square roots. (F) Average (diamonds) and standard deviation (error-bars) of the encoding rate density. While the averages are simply $\sum_i \mu_i^{(\pm)}$, the standard deviations are their theoretical value, $(\sigma_I^2 + \sigma_c^2)/w$. The inset shows the theoretical value (continuous lines), along with the numerical estimation of the rate standard deviation, by means of the Jack-Knife method [47], using an increasing sliding window Δ_J (abscissa). (G) Average (circles) and standard deviation (error-bars) of the readout neuron firing rate ($T_c = 100$ in simulations). The difference in the averages divided by the (stimulus-averaged) error is the SNR. In this figure, we estimated the standard deviation by means of the Jackknife error (inset ordinates) for increasing sliding window (inset abscissa), and taking the largest value. The simulation parameters are: $N = 2$, $\alpha_V = 0.9$, $\sigma_i = 12$, $\tau_c = 0.1$, $\tau_m = 0.05$, $\mu_I^{(-)} = 100$, $\mu_I^{(+)} = 120$, $w = 0.05$. See [48] and Appendix C for further details.

$$\mu_I^{(s)} = wN\bar{\mu}^{(s)} \quad (6a)$$

$$\sigma_I^{(s)2} = w\mu_I^{(s)} \quad (6b)$$

$$\sigma_c^2 = w^2 N \sigma_V^2 (1 + (N - 1)\alpha_V^2) \quad (6c)$$

where $\bar{\mu}^{(s)}$ and σ_V^2 are the average of current means and variances $\mu_i^{(s)}$ and $\sigma_{V_i}^2$ over encoding neurons i , respectively. For simplicity, in Eqs. (6) we consider a homogeneous gain vector $w_i = w \forall i$ (see Appendix B for a generalization to

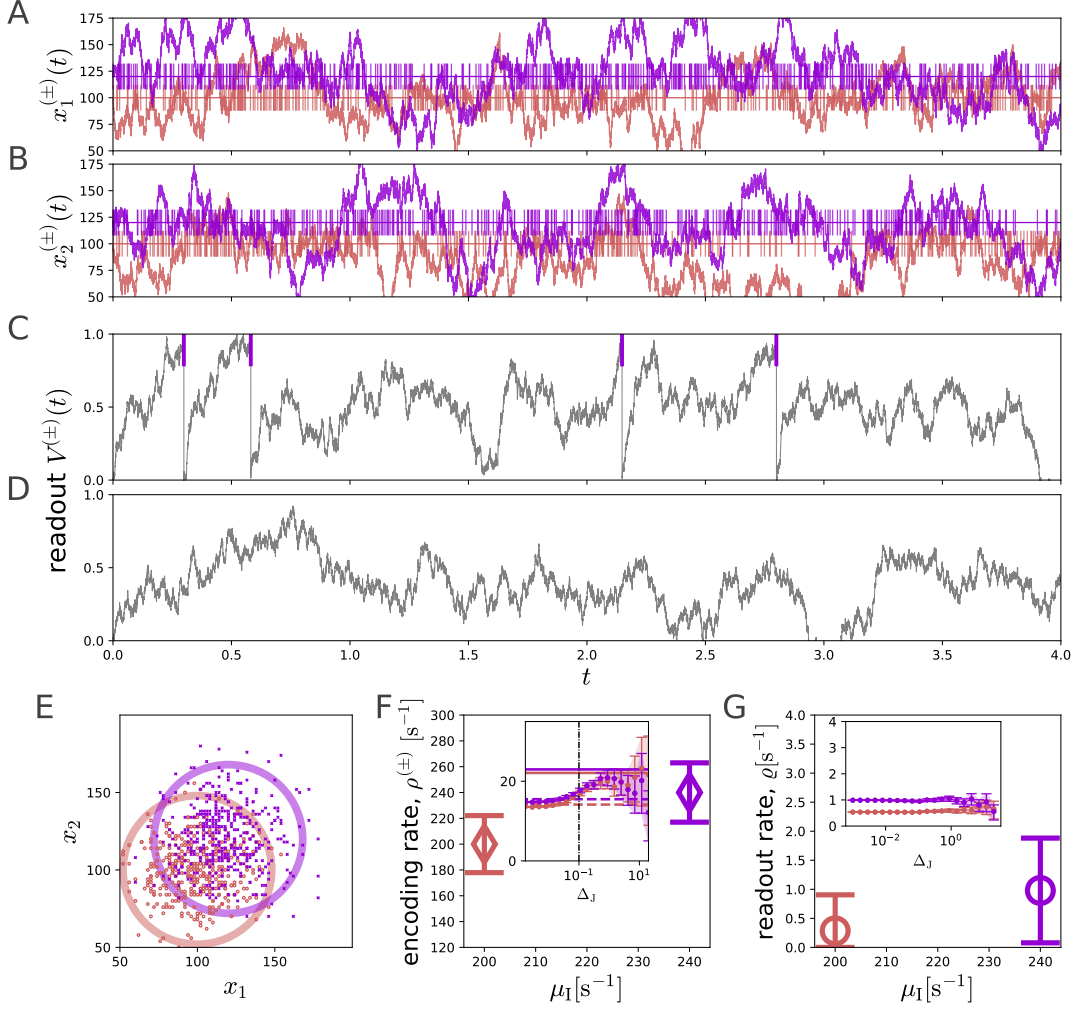


FIG. 3. *Neural activity in the neural encoding and readout model*, as in Fig. 2, but in absence of noise correlations $\alpha_V = 0$. Note the agreement between the numerical and theoretical rate standard deviation in panel F. Note as well that, even in absence of off-diagonal noise correlations $\alpha_V = 0$, the total firing rate $x^{(s)}(t)$ oscillates around its mean (because the diagonal of the noise correlation matrix is nonzero: $\sigma_c \neq 0$ even if $\alpha_V = 0$ in Eq. (6c)). We can see that the *encoding SNR* increases, with respect to the prevalence of noise correlations in Fig. 2 (since $\mu^{(+)} - \mu^{-}$ is constant, while σ_c has decreased). The rest of the parameters are: $N = 2$, $\alpha_V = 0$, $\sigma_i = 12$, $\tau_c = 0.1$, $\tau_m = 0.05$, $\mu_I^{(-)} = 100$, $\mu_I^{(+)} = 120$, $w = 0.05$.

arbitrary correlation matrices \bar{C} and gain vectors \mathbf{w}). The time-shifted covariance of the current $I(t)$ takes the form (from Eq. (5)):

$$\langle (I(t) - \mu_I)(I(t') - \mu_I) \rangle = \sigma_I^2 \delta(t - t') + v_c e^{-|t - t'|/\tau_c} \quad (7a)$$

$$v_c := \frac{\sigma_c^2}{2\tau_c} = w^2 N v_V (1 + (N - 1)\alpha_V^2). \quad (7b)$$

where v_c is the *stationary variance of the colored noise*.

In sum, while the encoding is in principle characterized by the $3N + 2$ parameters $\mu^{(\pm)}$, \mathbf{v}_V , α_V , τ_c , in the diffusion approximation it is described by the 4 parameters $\mu_I^{(\pm)}$, $v_c(\alpha_V)$, τ_c . The firing statistics of the readout depend on these encoding parameters and on the readout parameters w , τ_m (note that $\sigma_I^{(\pm)}$ is already determined by $\mu_I^{(\pm)}$, given w , see Eq. (6)).

Encoding signal-to-noise ratio. From Eq. (6c) it follows that the fraction of shared noise α_V increases the amplitude σ_c of colored correlations. In fact, in the unit time interval, the SNR of the input current $I(t)$ is given by (see Eqs. (7,11)):

$$\text{input SNR} = \frac{\mu_I^{(+)} - \mu_I^{(-)}}{\left(\sigma_c^2 + (\sigma_I^{(+)^2} + \sigma_I^{(-)^2})/2\right)^{1/2}} \quad (8)$$

which monotonically decreases with α_V (see Eq. (6c)).

In Appendix D we assess the validity limits of the diffusion approximation and its analogy with the non-Markovian random walk problem.

B. The quenched-noise approximation for the LIF neuron rate mean

In the following, we derive expressions for the mean and variance (and SNR, see Eq. 4) of the readout neuron defined by Eq. 5 as a function of the parameters $\mu_I^{(\pm)}$, v_c , τ_c , w , τ_m .

How to compute analytically the mean and variance of the firing rate of a LIF model with a coloured noise input has been extensively investigated. Approximate expressions for the mean r_R have been derived in the $\tau_c \ll \tau_m$ and $\tau_c \gg \tau_m$ limits [10, 16, 17, 19, 42, 45]. In particular, Moreno et al [17] derive an analytical approximation to the mean firing rate r_R of the colored-input noise LIF neuron in the $\tau_c \gg \tau_m$ limit (at first order in τ_m/τ_c), and under the further approximations of small $\alpha_M := \sigma_c^2/\sigma_I^2$ and small $\mu_I/(\sigma_I^2 + \sigma_c^2)^{1/2}$.

Here we present an approximated expression for r_R in the $\tau_c \gg \tau_m$ limit, in the *quenched-noise approximation*. The quenched-noise approximation generalizes the Moreno solution [17] to larger values of α_M . The approximation stands on a simple argument: whenever $\tau_c \gg \tau_m$, in time windows of length ℓ , $\tau_m \ll \ell \ll \tau_c$, the coloured noise $\xi(t)$ is approximately constant and, consequently, *the rate of the LIF neuron behaves as that of a white-noise LIF neuron* with input current $I(t) = \tilde{\mu} + \sigma_I \eta(t)$, where $\tilde{\mu} = \mu_I + \sigma_c \xi$ is an effectively constant drift. Under this assumption, the firing rate r_R in time intervals of size $T_c \gg \tau_c$ can be approximated as *the average of $r_w(\tilde{\mu})$ over the stationary distribution of values of $\tilde{\mu} \sim \mathcal{N}(\tilde{\mu}; \mu_I, v_c)$ with $v_c = \sigma_c^2/(2\tau_c)$* (see (Eq. 5)), where $\mathcal{N}(\cdot; m, v)$ denotes the normal distribution with mean m and variance v . Thus, the readout firing rate in the quenched-noise approximation $r_R(\mu_I) \simeq r_q(\mu_I)$ is given by:

$$r_q(\mu_I) := \langle r_w(\tilde{\mu}) \rangle_{\mathcal{N}(\tilde{\mu}; \mu_I, v_c)} \quad (\text{quenched-noise approximation}) \quad (9)$$

where $r_w(\mu)$ is the Siegert solution for the mean rate of a *white noise LIF neuron* (see Eq. (E2) in Appendix E) [42, 46]. In the saddle-point approximation for large τ_c/τ_m (see Appendix E) we have:

$$r_q(\mu_I) = r_w(\mu_I) \left[\frac{1}{1 - v_c g'_1(\mu_I)} \right]^{1/2} \exp \left(\frac{v_c}{2} \frac{g_1^2(\mu_I)}{1 - v_c g'_1(\mu_I)} \right) \quad (10)$$

where the function $g_1 := r_w'/r_w$ and its derivative g'_1 with respect to μ_I depend on the white LIF neuron parameters only. Notice that, consistently with the quenched-noise hypothesis in Eq. (9), the emerging correction to the white noise case depends on the properties of the colored noise only through v_c .

Interestingly, if we now expand $[1 - v_c g'_1(\mu_I)]^{-1/2}$ in (Eq. 10) to the first order in $\nu_W = (\sigma_c^2 \tau_m)/(\sigma_I^2 \tau_c)$ (W stands for Walter et al, who use the same perturbative parameter in reference [49]), and the exponential in (Eq. 10) to the first order in τ_m/τ_c , we recover the Moreno et al expression for r_R at first order in τ_m/τ_c in Eq. (E1). This is therefore a generalization of the Moreno solution for r_R in the $\tau_c \gg \tau_m$ limit [17, 19], expected to hold for larger values of α_M (Figs. 4,8-A and Appendix F).

Comparing the Moreno [17] and quenched-noise approximations with the numerical data in the limit $\tau_c \gg \tau_m$ reveals that: (i) for low σ_c both approximations r_M and r_q converge to the white-noise LIF activation function r_w (Eq. (10)) and for low enough σ_c and hence α_M , both solutions r_M and r_q are consistent with each other (Fig. 4-A red lines, Fig. 8-A and Appendix F); (ii) for larger values of σ_c the solutions differ, and the numerical estimation of r_R (i.e. \tilde{r}_R ; see Appendix C), is *consistent only with the quenched-noise approximation* (Fig. 4-B blue lines); (iii) to find *full agreement* between numerical simulations and r_q , we need to apply the finite-Number of Integration Steps (NIS) correction (Fig. 4-B, see Appendix C).

C. Intuitive interpretation of the enhanced firing rate effect in the quenched-noise approximation

The quenched-noise approximation provides us with an intuitive interpretation of the enhancement of the firing rate in the presence of colored noise. Since $r_q(\mu_I) \simeq \langle r_w(\tilde{\mu}) \rangle_{\tilde{\mu}}$ (Eq. (9)), we expect the introduction of a colored

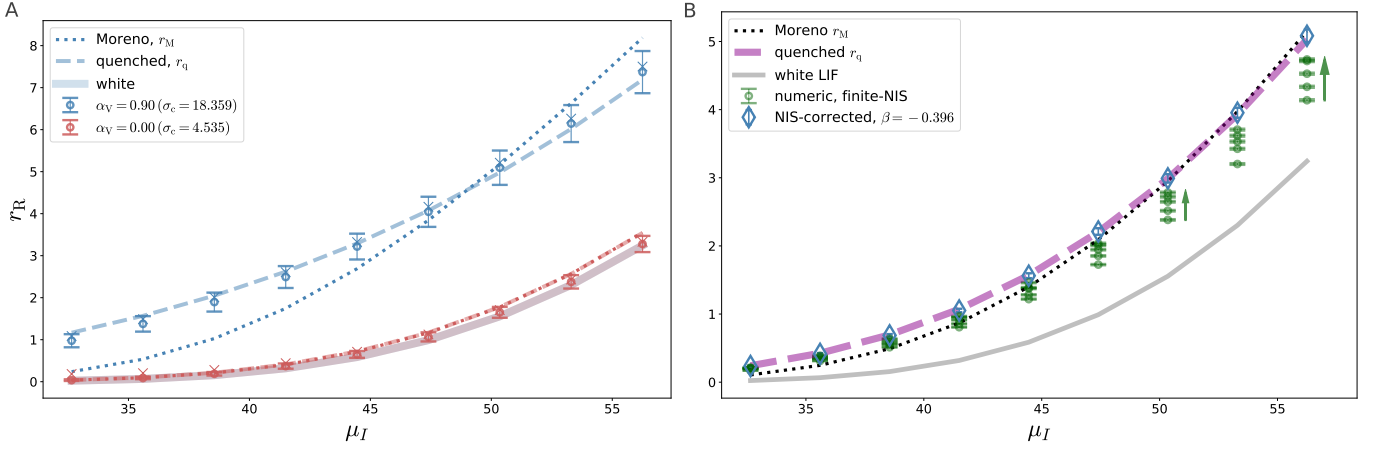


FIG. 4. *Readout firing rate r_R vs μ_I : numerical estimations and analytical approximations.* (A) r_R vs μ_I for two values of the noise correlation alignment: $\alpha_V = 0$ (no noise correlations, red curve), and $\alpha_V = 0.9$ (strong information-limiting noise correlations, blue curve). The numerical estimation (points) correspond to a simulation with the highest NIS, $n_{is} = 2^{17}$ (see Appendix C). The error-bars are the rate standard deviation in the unit time window, $(v_R \times T_c)^{1/2}$, estimated as the standard deviation of the spike count $n_R(T_c)$ in $[0, T_c]$ across $n_{tr} = 10^3$ simulation trials. The analytical activation functions corresponding to the white-noise LIF, $r_w(\mu_I)$ in (E2), the Moreno solution $r_M(\mu_I)$ for $\tau_c \gg \tau_m$ in Eq. (E1) [17], and the quenched-noise approximation r_q in Eq. (9), are shown. The simulation parameters are: $\tau_c = 0.1$, $\tau_m = 0.005$, $\sigma_V = 1.778$, $w = 0.450$, $v_V = 25.39$. (B) Numerical estimations of r_R vs μ_I for $\tau_c \simeq 0.720$, and all the values of the NIS, $n_{is} = 2^m$ for $m = 12, \dots, 17$ (different green points at a common abscissa indicate different values of the NIS). The error-bars indicate the estimation $(\tilde{v}_R T_c)^{1/2}$. We report as well the finite-NIS corrected estimation of $\tilde{r}_R(\mu_I)$ (blue diamonds) and their error in the regression (error-bars), as well as the analytical approximations r_M and r_q . The finite-NIS corrected estimation is compatible with the quenched-noise approximation only. See Appendix C for details, and more on the comparison between the raw numerical, NIS-corrected numerical, Moreno, quenched-noise in Appendix F. The simulation parameters are: $\tau_c = 0.720$, $\sigma_c = 30.593$, $\tau_m = 0.005$, $w = 0.45$, $v_V = 9.8$.

noise to increase the LIF firing rate, $r_R(\mu_I) > r_w(\mu_I)$, for those values of μ_I in which r_w is convex, and vice-versa – since $\langle f(\mu) \rangle_\mu > f(\langle \mu \rangle_\mu)$ is the definition of convex function. Precisely, since $v_c^{1/2}$ is the standard deviation of $\tilde{\mu}$, we expect $r_q(\mu_I) > r_w(\mu_I)$ to hold for values of μ_I and v_c such that μ_I is lower, in units of $v_c^{1/2}$, than the inflection point μ^* of the white-noise LIF neuron (satisfying $d^2 r_w(\mu)/d\mu^2|_{\mu^*} = 0$). Fig. 5 shows that this is the case for both the quenched-noise and the Moreno approximations.

The enhancement in firing rate therefore has a simple explanation in the large-correlation timescale regime. The input current signal $I(t)$ fluctuates within a timescale τ_c . Although those fluctuations are symmetric around the mean μ_I , since the activation function of the white LIF model is non-linear, and convex for low enough current μ_I , the gain in firing rate for positive fluctuations, $r_w(\mu_I + \delta) - r_w(\mu_I)$ is larger than the loss for negative fluctuations $-r_w(\mu_I - \delta) + r_w(\mu_I)$. Thus, for the firing rate to be enhanced by colored noise, the LIF readout neuron must operate in a sufficiently low input current regime (so that $r_w(\mu_I)$ is convex, given the relevant parameters σ_I, τ_m , see Sec. V). This effect is known as *Jensen's force* in the literature [50].

D. The quenched-noise approximation for the LIF neuron rate variance

To our knowledge, the rate variance v_R of a LIF neuron with white+coloured noise input can be analytically computed only in the $\tau_c \rightarrow 0$ limit [12], in the $\tau_c \rightarrow \infty$ limit with no white noise [21], for a perfect integrator [18, 20], for conductance synapses [14], for binary-valued inputs [15] or for oscillating, periodic input [13]. In any case, there are no closed analytical expressions for the problem at hand (see also [22]) [51]. Here we derive an expression for the rate variance within the quenched-noise approximation.

We first provide an expression for the *temporal correlation function* $C(t) := \langle \varrho(t') \varrho(t' + t) \rangle - \langle \varrho(t') \rangle \langle \varrho(t' + t) \rangle$ of a LIF neuron with white+colored input noise (Eq. (5)) in the quenched-noise approximation (where $\varrho(t) := \sum_j \delta(t - t_j)$ is the LIF spike density in a single realization, and $\langle \cdot \rangle$ is the average over realizations of the noises ξ, η). The rate variance $\text{Var}(\text{rate}) = T_c^{-2} \text{Var}(n_R(T_c))$ relates to C as:

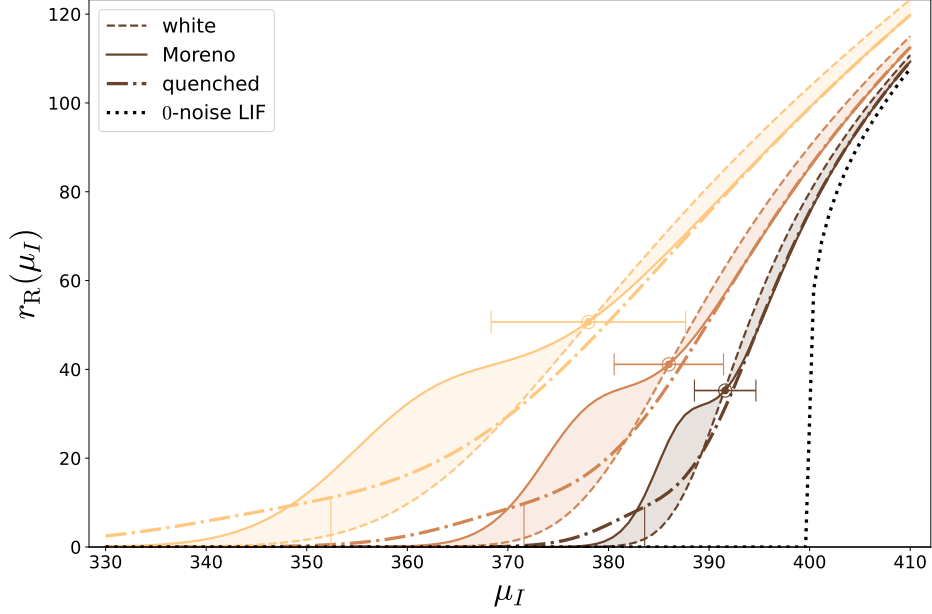


FIG. 5. *Activation function of the LIF neuron with white and colored input noise.* The dashed lines denote the Siegert expression for the white-noise LIF $r_w(\mu_I)$; the continuous curves are the Moreno solution (E1) for $\tau_c \gg \tau_m$; the dashed-dotted lines are the quenched-noise approximation in (9); the black dotted line is the LIF activation function in the absence of noise, $r_0(\mu) = [-\tau_m \ln(1 - (\mu\tau_m)^{-1})]^{-1}$. Different colors correspond to different values of the gain $w = (0.00031, 0.001, 0.00316)$ (from darker to lighter). The rest of the parameters are: $\tau_m = 2.5 \cdot 10^{-3}$, $\tau_c = 10^{-1}$, $\sigma_I^2 = w\mu_I$, $\sigma_c = 8\bar{\sigma}_I$, with $\bar{\sigma}_I^2 = w\bar{\mu}_I$ and $\bar{\mu}_I = 370$. The circles over the curves show the inflection point of the white-noise LIF neuron, and error-bars indicate $v_c^{1/2}$ in every direction.

$$\text{Var}(\text{rate}) := v_R = \frac{r_R}{T_c} + \frac{2}{T_c^2} \int_0^{T_c} dt'(T-t')C_-(t') \quad (11)$$

where $C_-(t)$ is the regular part of $C(t) = r_R\delta(t) + C_-(t)$. We define as well the *temporal distribution function* $g(t) := r_R^{-1} \langle \varrho(t')\varrho(t'+t) \rangle$, i.e. the spike density at a distance t from each spike, so that $C(t) = r_R g(t) - r_R^2$.

We compute $g_q(|t-t'|)$ in the quenched-noise approximation (Appendix G) by using the facts that (i) the effective encoding current $\tilde{\mu}_t := \mu_I + \sigma_c \xi(t)$ (III A) obeys an Ornstein-Uhlenbeck process (Eq. (5)) with known stationary distribution $p(\tilde{\mu}_t) = \mathcal{N}(\tilde{\mu}_t; \mu_I, v_c)$, and Green function, $p(\tilde{\mu}_{t'}|\tilde{\mu}_t)$; (ii) in the quenched-noise approximation we have that $r_q g_q(t-t') \simeq \langle \langle r_w(\tilde{\mu}_t) r_w(\tilde{\mu}_{t'}) \rangle \rangle_{p(\tilde{\mu}_{t'}|\tilde{\mu}_t)} \langle p(\tilde{\mu}_t) \rangle$. Thus, our derivation addresses the impact of pre-synaptic current fluctuations in the post-synaptic *temporal correlations*, beyond their impact in the post-synaptic mean firing rate. The resulting expression for $g_q(|t-t'|)$ is expected to be valid for resolution timescales ℓ satisfying $\tau_m \ll \ell \ll \tau_c \ll T_c$ and for low $\omega := \exp(-|t-t'|/\tau_c)$ and is given by (Appendix G):

$$r_R g_q^{(\text{low-}\omega)}(t-t') \simeq r_q^2 \left(1 + e^{-|t-t'|/\tau_c} Q \right) \quad \text{for large } |t-t'|/\tau_c \quad (12)$$

where Q is a constant that depends on the white LIF properties μ_I, σ_I, τ_m , and on v_c (see Eq. (G14) in Appendix G).

The comparison with the numerical estimation of g (Appendix C) reveals that Eq. (12) captures the behavior of the distribution function for large t (Fig. 6). Although the quenched-noise approximation is expected to be valid for resolution timescales $\ell \gg \tau_c$, g_q reproduces well the numerical g 's even at small values of t of the order of τ_c (colored vertical lines in Fig. 6) and even as small as the zero-noise LIF ISI μ_I^{-1} (black vertical line in Fig. 6).

We can exploit our expression for $g_q^{(\text{low-}\omega)}$ to draw two approximations for the rate variance (see Fig. 6), depending on the value of a temporal cutoff t_0 .

The first approximation is an upper bound, computed from Eq. (11) but taking $g(t)$ to be equal to our low- ω expression for g_q in Eq. (12) for all times $0 < t < T_c$. The area below this upper bound is the green, slash-hatched area in Fig. 6, which is an upper bound for the integral of g (shadowed violet area below the g curve in the figure). This upper bound is given by $v_q \simeq r_R T_c^{-1} + 2T_c^{-2} \int_0^{T_c} dt'(T-t')C_-^{(\text{low-}\omega)}(t')$.

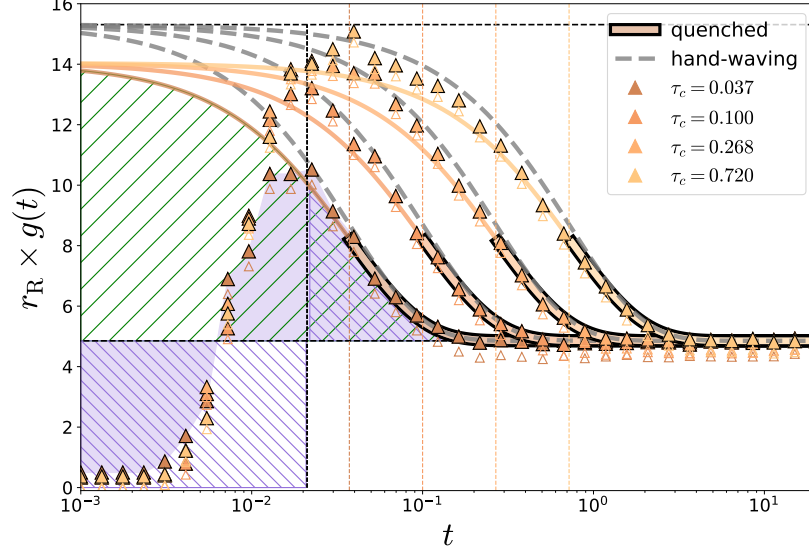


FIG. 6. *Temporal distribution function $g(t)$ of readout spikes.* Different curves/colors correspond to different values of τ_c . The points correspond to the numerical estimation from the simulated spike trains (see Sec. C); the colored continuous curves correspond to the quenched approximation g_q in (12) (please, note that these curves become bordered by a black line for $t > \tau_c$, in the regime in which they have been derived). Importantly, in order to correct the finite-NIS effect, we have shifted the numerical g points by a quantity, τ_c -dependent but constant in μ_I , which is $-\tilde{r}_R + r_q$, where $-\tilde{r}_R$ is the numeric estimation of the rate (which is underestimated, due to the finite-NIS effect). To show the effect of such a shift, we report as well the raw, non-shifted numerical estimations (small, void triangles). The gray dashed lines are the hand-waving expression for g , (H1) in Appendix. H. The dashed and continuous horizontal lines mark, respectively, the values $v_q + r_q^2$ and r_q^2 . The black vertical line signals μ_I^{-1} , while the vertical colored lines mark the corresponding values of τ_c . It is interesting to note that the hand-waving approximations for g seem to work slightly worst than g_q , as expected. The parameters of the simulation are: $\mu_I = 47.4$, $\alpha_V = 0.9$, $v_V = 9.8$, $v_c = 650.22$, $\sigma_I = 4.618$.

The second approximation is a lower bound, computed from Eq. (11) but taking $g(t)$ to be equal to the low- ω expression for g_q in Eq. (12), only for a given temporal range $t > t_0$, while being equal to 0 for $t \leq t_0$. The area below this lower bound is the blue, backslash-hatched area in Fig. 6, which is a lower bound for the integral of g . This lower bound is given by $v_q \simeq \frac{r_R}{T_c}^{-1} + 2T_c^{-2} \int_{t_0}^{T_c} dt' (T - t') C_-^{(\text{low}-\omega)}(t') - r_R^2 \left(\frac{t_0}{T_c} - \frac{t_0^2}{2T_c^2} \right)$.

As seen in Fig. 6, in the upper bound approximation we overestimate the refractory period of g (in which $g < r_q < g_q^{(\text{lo}-\omega)}$) for low enough times $t < t_0$. In fact, our approximation is not expected to capture the behavior of g in timescales of the order of τ_c or lower. Vice-versa, the lower bound approximation underestimates the low- t behavior of g , since g is set to its minimum possible value, $g(t) = 0$ for $t < t_0$. For the lower bound to work, the cutoff time t_0 must be close to the maximum of the function g . As a natural guess, we choose it to be $t_0 = \mu_I^{-1}$, the zero-noise LIF ISI (see Fig. 6).

In short, taking $C_-^{(\text{low}-\omega)}(t') := r_q g_q^{(\text{lo}-w)} - r_q^2$, with $g_q^{(\text{lo}-w)}$ in Eq. (12), our upper- and lower-bound expressions for the rate variance take the form:

$$v_q \simeq \frac{r_R}{T_c} + 2r_R^2 Q \frac{\tau_c}{T_c} \quad \text{upper bound} \quad (13a)$$

$$v_q \simeq \frac{r_R}{T_c} + 2r_R^2 Q \frac{\tau_c}{T_c} \left(e^{-\frac{t_0}{\tau_c}} - e^{-\frac{T_c}{\tau_c}} \right) - r_R Q \frac{\tau_c^2}{T_c^2} \left[e^{-\frac{t_0}{\tau_c}} \left(\frac{t_0}{\tau_c} + 1 \right) - e^{-\frac{T_c}{\tau_c}} \left(\frac{T_c}{\tau_c} + 1 \right) \right] + \\ - r_R^2 \left(\frac{t_0}{T_c} - \frac{t_0^2}{2T_c^2} \right) \quad \text{lower bound.} \quad (13b)$$

These approximations capture the rate variances in a broad range of μ_I and τ_c parameters (see Fig. 7 and Appendix F). In particular, the quenched-noise approximation to the variance in Eq. (13) captures both the negative deviations from Poissonian noise $\text{Var}(\text{rate}) = r_R/T_c$ (that originate from the refractory period for $t > t_0$, $C(t) < 0$), and the

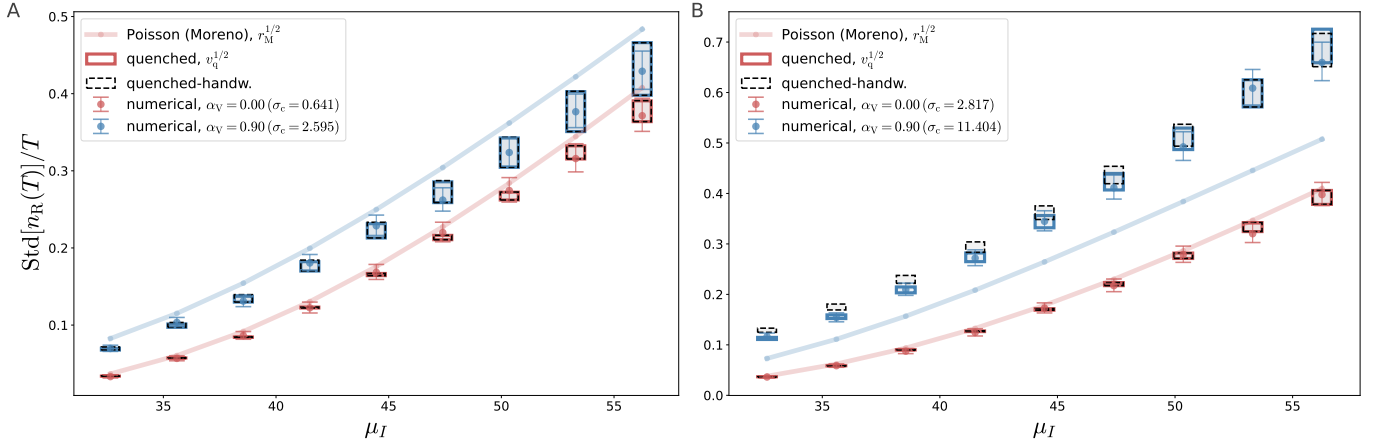


FIG. 7. Standard deviation of the firing rate in the unit time interval, $\text{Std}(\text{rate}) T_c^{1/2} = (v_R T_c)^{1/2}$, vs μ_I . Different panels correspond to two simulations with different values of τ_c ($\tau_c = 0.0052$ and 0.1 for panels A and B respectively). Different curves in each panel correspond to different values of $\alpha_V = 0, 0.9$: absence of noise correlations, and highly aligned noise correlations, respectively. The points are the numerical estimations: standard deviations of $n_R(T_c)/T_c$ across the n_{tr} trials ($\times T_c^{1/2}$). The error-bars are the confidence interval of the corresponding χ^2 variance, with a probability $\alpha_\chi = 0.9$ (see Appendix C). Continuous lines are the Poisson-quenched hypothesis $v_R = r_q/T_c$; the filled, continuous-line boxes are our quenched-noise upper and lower bounds for the variance (13) (upper and lower limits of the box); the void, dashed-line boxes correspond to the upper and lower bounds in the hand-waving approximation (see Appendix H). We observe that in absence of noise correlations when $\alpha_V = 0$, the Poisson approximation is relatively good, specially for low μ_I . Only large values of σ_c induce positive corrections of the Poisson variance. The quenched-noise approximation captures both negative and positive deviations from Poissonian variance. The rest of the parameters are: $\tau_m = 0.005$, $w = 0.450$, $\sigma_V = 1.104$.

over-Poissonian deviations (originating from the high- t regime, in which $C(t) > 0$).

In Appendix H, we develop a further approximation to the firing rate variance, that we will refer to as *hand-waving approximation*, and which admits a straightforward interpretation of the over-Poissonian enhancement.

IV. NOISE CORRELATIONS AND SNR ENHANCEMENT IN THE ENCODING-READOUT MODEL

In this section, we study the behavior of the SNR of the readout (Eq. 4) as a function of the noise correlation stationary variance v_c (parametrised by α_V) and timescale τ_c . Crucially, for the comparison between numerical estimations and theoretical approximations for different values of τ_c , we keep the *noise stationary variance v_c constant and independent on τ_c* , which amounts to consider a τ_c -dependent count variance $\sigma_c^2 = 2\tau_c v_c$ (see [21]). Taking v_c constant is the suitable scenario to explore the $\tau_c \gg \tau_m$ limit without loss of generality (see Appendix J), which allows us to employ the quenched-noise approximation for the LIF model rate mean and variance, valid in the $\tau_c \gg \tau_m$ limit.

In IV A we first study the behavior of the SNR by comparing the numerical simulations with the following analytical approximations.

For the colored-noise LIF rate r_R we will use: *the two Moreno approximations* [17] r_M for the firing rate, expected to hold in the limits $\tau_c \ll \tau_m$ and $\tau_c \gg \tau_m$ (Eq. E1), respectively, and for low α_M and low $\mu_I^2/(\sigma_c^2 + \sigma_I^2)$; and *the quenched-noise approximation* r_q in Eq. (9), expected to hold for $\tau_c \gg \tau_m$ and for low $\mu_I^2/(\sigma_c^2 + \sigma_I^2)$.

For the colored-noise LIF variance v_R we will use: (i) *The Poisson approximation* $v_R \simeq r_R/T_c$, consisting in neglecting the time-correlated part of the temporal correlation C_- in Eq. (11). This approximation works relatively well in the absence of noise correlations ($\sigma_c = 0$), and for low values of μ_I . Then, the mean rate can be approximated with the Moreno expression $r_R \simeq r_M$ (*Poisson-Moreno approximation*); and (ii) *The quenched-noise approximation* for the variance, v_q in Eq. (9), expected to hold for $\tau_c \gg \tau_m$ and for low $\mu_I^2/(\sigma_c^2 + \sigma_I^2)$.

A. Signal enhancement, noise enhancement and SNR enhancement

1. Signal enhancement

We now present the numerical results for the readout mean rate enhancement $\Delta r_R := r_R^{(+)} - r_R^{(-)}$ versus τ_c , for two values of the fraction of shared noise α_V (see Appendix C for the numerical range of probed parameters, and Appendix F for different choices of such parameters).

First, we observe that introducing noise correlations enhances the firing rate difference for all the considered values of τ_c (Fig. 8-A). This effect is not simply equivalent to the *LIF neuron firing rate enhancement in the presence of noise correlations* (see Fig. 4), but it corresponds to an increase of the mean firing rate *difference* Δr_R , in the presence of noise correlations.

For low enough τ_c (and constant $v_c = \sigma_c^2/(2\tau_c)$), the colored-noise amplitude σ_c vanishes, so that the numerical Δr_R is consistent with that of the white noise LIF Δr_w . For larger but low enough values of τ_c , the Moreno perturbative approximation to r_R for low τ_c/τ_m holds as expected. For large values of $\tau_c \gg \tau_m$, we observe a disagreement between the numerical estimation and the Moreno approximation, and an agreement between the numerical estimation and the quenched-noise approximation, as expected (see Sec. IIIB and Appendix F) [52]. For intermediate values of $\tau_c \lesssim \tau_m$, although outside the validity limits of both approximations, we observe a nice agreement between the numerical Δr_R and the interpolation of both Moreno solutions [17] (although this agreement is sensitive to the interpolating time, here set to $t_{in} = 2.5\tau_m$).

Thus, for fixed values of the parameters $\mu_I^{(\pm)}$, τ_m , w , increasing noise correlations leads to an increase in the readout neuron firing rate difference Δr_R , quantitatively understood within the Moreno et al solution for low τ_c and within the quenched-noise approximation (Sec. IIIB) for large enough τ_c .

As a methodological note, the numerical simulations match the analytical predictions only when applying the finite-Number of Integration Steps (NIS) correction to the numerical solution of the stochastic differential equation, Eq. 5) (see Appendix C).

2. Rate variance enhancement

We now consider the denominator of the SNR, i.e. the stimulus-averaged variance of the readout firing rate, $(v_R^{(+)} + v_R^{(-)})/2$. First, for low enough τ_c we observe an agreement between \tilde{v}_R and the Poisson-Moreno approximation (Fig. 8-B). We attribute small deviations to a numerical underestimation of the variance due to the finite-NIS effect (Appendix K). We notice that in this case we do not employ the NIS-corrected estimation for the rate variance, since it exhibits larger statistical errors. Second, the increment of \tilde{v}_R for large values of τ_c in the presence of noise correlations can be explained, within the quenched-noise approximation, as the result of the integration of the over-Poissonian part of the temporal correlation function g_q (see Eq. (13), and Appendix H for a further, intuitive explanation of the enhancement of \tilde{v}_R for large τ_c).

Overall, the Poisson-Moreno and quenched-disorder approximations for v_R describe the numerical \tilde{v}_R in the $\tau_c \ll \tau_m$ and $\tau_c \gg \tau_m$ regimes, respectively. For large τ_c the variance v_R increases with τ_c (see the second term in Eq. (11) and Eq. (13)), while the mean rate r_R stays constant with τ_c (see Eq. (10)).

3. SNR enhancement

From the results of the previous sections, it follows that the SNR exhibits a non-monotonic behaviour with τ_c (Fig. 8-C). For large enough τ_c , noise correlations lower the readout SNR below its value in absence of noise correlations. For high values of τ_c , the increment of the SNR numerator, Δr_R , depends only on v_c , so that it stays constant in τ_c (see Fig. 8-A and Sec. IIIB). Instead, the rate variance increases with τ_c due to the over-Poissonian correction (which increases with *both* τ_c and v_c , see Eq. (13a) and Appendix H). Beyond a certain value of τ_c , the increment in the denominator becomes prevalent, thus leading to a decrement of the SNR. For sufficiently small τ_c , when the enhancement in the rate variance $(v_R^{(+)} + v_R^{(-)})/2$ is not enough to overcome that of Δr_R in the SNR numerator, we observe that the noise correlations induce an enhancement of the SNR. This constitutes the apparently paradoxical effect according to which encoding correlations that lower the encoding-SNR enhance the readout SNR.

In Fig. 8-C we report as well the *encoding SNR* (see Eq. (8)), which, by construction, decreases with the noise correlation amplitude, and which may actually become lower than the readout SNR (please, see a discussion on this point in Appendix I).

For details regarding the small theoretical-numerical disagreement for low τ_c in Fig. 8-C, we refer to the Appendix K, where we attribute it to the finite-NIS effect.

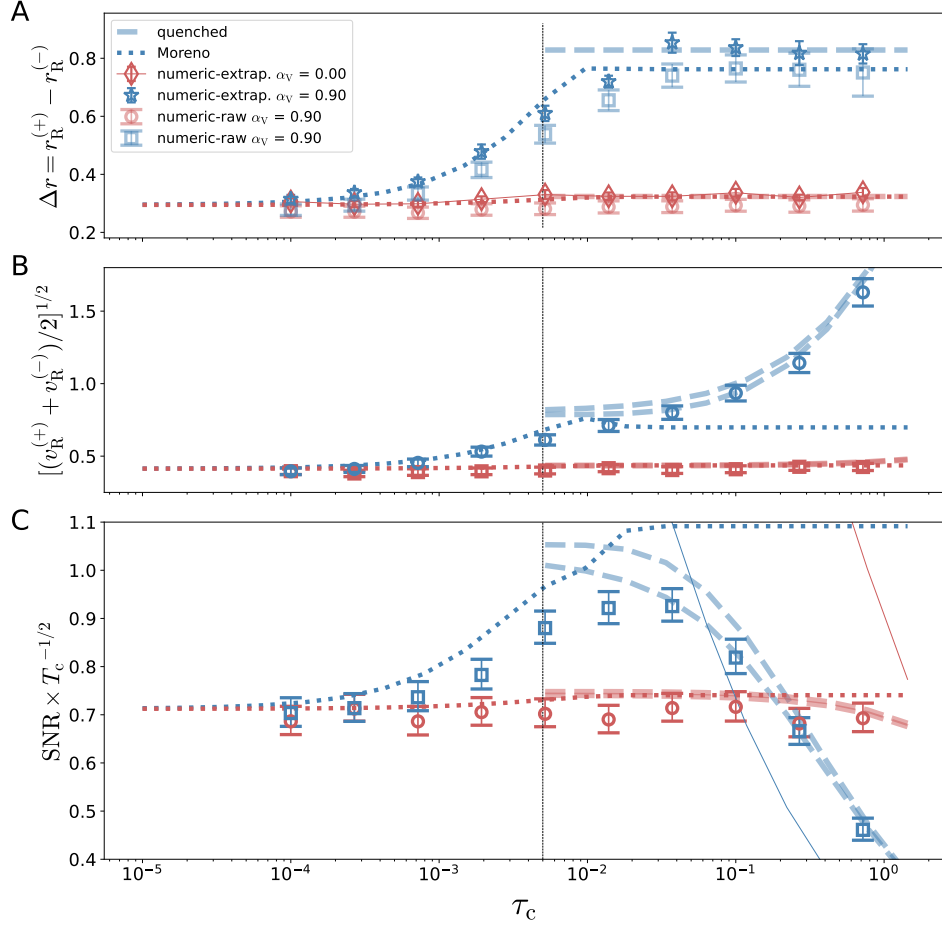


FIG. 8. *Mean rate enhancement, rate standard deviation and SNR, as a function of τ_c .* (A) Readout mean rate increment $\Delta r_R = r_R^{(+)} - r_R^{(-)}$ vs τ_c . Different curves/colors in each panel correspond to both values of $\alpha_V = 0, 0.9$. Void points correspond to the infinite-NIS extrapolated procedure (see Appendix C) (and the error-bars indicate the uncertainty of the regression), while the semi-transparent points correspond to the raw numerical estimations \tilde{r}_R for the highest NIS (and the error-bars are $(\tilde{v}_R T_c)^{1/2}$). The dashed lines are the interpolated Moreno perturbative solution in [17], using an interpolating time $t_{in} = 2.5\tau_m$. The continuous line (shown for $\tau_c > \tau_m$ only) is the quenched-noise value, Eq. (9). The vertical dotted line signals the value of τ_m . (B): Standard deviation of the stimulus-averaged readout firing rate in the unit time interval, $[(v_R^{(+)} + v_R^{(-)})/2]^{1/2} T_c^{1/2}$ vs τ_c . Here, only the raw estimations of the variance are shown (filled points). The error-bars are the χ^2 confidence interval with a probability $\alpha_\chi = 0.95$. The pairs of dashed lines (shown for $\tau_c > \tau_m$ only) correspond to the lower and upper bounds for the variance in the quenched-noise approximation, (13). We attribute the slight disagreement between the numerical estimations and v_q to a finite-NIS underestimation of the numerical variance. (C): Readout SNR in the unit time interval (of which panels A and B are, respectively, the numerator and the denominator), vs τ_c . The numerical points correspond to the raw estimators for both the numerator and the denominator. The thin dotted lines are the *encoding* signal-to-noise ratio in the unit time interval, Eq. (8). The simulation parameters are: $(\mu_I^{(+)}, \mu_I^{(-)}) = (32.65, 41.5)$, $w = 0.45$, $v_V = 9.80$.

In sum, the SNR presents a non-monotonic behavior with τ_c , that is quantitatively explained by the quenched-noise approximation (and, for low τ_c , by Moreno et al approximation to $o(\tau_c/\tau_m)$).

B. The conditions for enhanced-by-consistency SNR to occur

In this section we address *for which general values* of the encoding and decoding parameters we expect the SNR enhancement to occur in the presence of noise correlations. The quenched-noise approximation for the rate mean and variance allows us to draw necessary conditions on the NERM parameters, at least for sufficiently large τ_c . Our conclusions are drawn from the behavior of r_q, v_q as a function of μ_I and σ_c (Fig. 9). In this section, we use the

quenched-noise approximation and, in particular, the hand-waving expression for the rate variance, Eq. (H4) in Appendix G, which is already a good approximation for the behavior of the rate variance (Fig. 7).

Conditions on $\mu_I^{(\pm)}$. We said that, for the colored noise to enhance *the firing rate* r_R , the value of μ_I should be safely lower than the inflection point of the LIF (circle in Fig. 9-A, see Sec. III C). Given the parameters of the white LIF τ_m, σ_I , the inflection point occurs at the value of μ_I for which $g_1^2 + g_1' = 0$, where $g_1 = r_w'/r_w$. The inflection point μ_I^* of $r_w(\mu_I)$ is also the value of μ_I below which $r_q > r_w$ for low enough v_c (indeed, expanding r_q in (10) to $o(v_c)$, we get that $r_q \geq r_w$ for $\mu_I \leq \mu_I^*$, v. Fig. 9). Since the SNR numerator is $\Delta r_R \leq r_R(\mu_I^{(+)})$, a necessary condition for the SNR to be positive is $\mu_I^{(+)} < \mu_I^*$. We can make this condition more stringent by imposing that, beyond the numerator, the SNR itself should increase. The numerator $r_R^{(+)}$ and the denominator $v_R^{(+)}$ both increase with σ_c , so that both effects cancel at first order in v_c . In fact, to order $o(v_c)$, the condition $\text{SNR}_q = \text{SNR}_w = r_w^{1/2}$ translates into $g_1' + g_1^2 = 2\tau_c r_w g_1^2$, implying that the value of μ_I , say $\hat{\mu}_I$ (green line in Fig. 9), for which this relation is satisfied *does not depend on v_c* . Indeed, the μ_I value at which the SNR becomes positive depends slowly on σ_c (Fig. 9). Therefore, the condition, $\mu_I^{(+)} < \hat{\mu}_I$ can be taken as a *necessary condition on $\mu_I^{(+)}$* for the SNR to increase in the presence of noise correlations, in the NERM (and for large enough $\tau_c \gtrsim \tau_m$). This necessary condition is, of course, not sufficient to guarantee that $\text{SNR}_q > \text{SNR}_w$, since so far we have neglected $r_R^{(-)}$ in front of $r_R^{(+)}$. Non-negligible values of $r_w(\mu_I^{(-)})$ (hence, of $r_R^{(-)}$) may change this scenario (Fig. 21 in Appendix L). The larger $\mu_I^{(-)}$, the lower Δr_R and, for low values of $\mu_I^{(-)}$, the larger $v_R^{(-)}$ as well.

For larger values of σ_c , the (leftmost) inflection points of r_w and v_R occur at lower values of μ_I (Fig. 9), implying that $\mu_I^{(-)}$ should take even lower values for the SNR to increase. For large enough values of σ_c (or v_c), the SNR denominator increases faster with σ_c than the numerator, because of the over-Poissonian correction to the variance, cf. the second term in Eq. (13a), or Eq. (H4) in Appendix H. This is the origin of the non-monotonous dependence of the SNR on the noise amplitude.

In sum, we derived *a set of necessary conditions* on $\mu_I^{(\pm)}$ for the SNR to increase, for large enough τ_c , and when the rest of the variables are kept constant, is: (c1) $\mu_I^{(+)} < \hat{\mu}_I$, and (c2) that $\mu_I^{(-)} < \hat{\mu}_I^{(-)}$ is low enough, with the upper bound $\hat{\mu}_I^{(-)}$ being a decreasing function of σ_c . The larger the amplitude of noise correlations, the larger should be the length of the current gap $\Delta\mu_I$ for the SNR to increase with noise-correlations.

Conditions on other variables. These considerations are enough to understand the qualitative dependence of the SNR with respect to the rest of the LIF parameters. We exemplify such dependencies in Fig. 10 and in Figs. 23,24,25 in Appendix M.

In general, we observe a non-monotonous behavior in both τ_c and $\Delta\mu_I$. The first one is the behavior that we described in Sec. IV A. The non-monotonous behavior in $\Delta\mu_I$ occurs since, for low input rate increment, the readout rate increment is negligible, while for too large increment $\mu_I^{(+)}$ approaches $\hat{\mu}_I$, and we loose the necessary condition for the SNR to increase.

In Fig. 10 we see how the SNR contour plots change with the value of $\mu_I^{(-)}$. For low enough $\mu_I^{(-)}$, the signal increment is essentially given by $r_R^{(+)}$, and the picture is as in Fig. 9: increasing $\mu_I^{(-)}$ and $\Delta\mu_I$ by the same quantity, leads to the same value of the SNR. The consequence is that increasing $\mu_I^{(-)}$ has the same effect of a shift in the y-axis (Figs. 10-A,B). However, beyond a certain value of $\mu_I^{(-)}$, $r_R(\mu_I^{(-)}) > r_w(\mu_I^{(-)})$ is no longer negligible, and increasing $\mu_I^{(-)}$ amounts to reduce Δr_R , to increase $v_R^{(-)}$ and, consequently, to a reduction of the SNR (Fig. 10-C, and Fig. 21 in Appendix L).

With similar arguments one can explain the qualitative dependence of the SNR on τ_m , w and σ_c (see Appendix M).

V. DISCUSSION

Here we used an Neural Encoding and Readout Model (NERM) of neural activity that combines information encoding in neural populations with a biophysically plausible model of neural readout, to investigate the conditions under which correlations between the temporal activity of input neurons can enhance the transmission of neural information downstream, even if they decrease the amount of information encoded in the input. Addressing this problem is highly relevant in neuroscience because it establishes theoretical grounds for the empirical and seemingly paradoxical discovery that higher correlations in neural activity aid performance at the behavioral level, even when they decrease the information at the encoding stage.

We formally analyzed a mechanism of enhanced-by-consistency readout proposed in [32], in which the readout is implemented as a single neuron with an output coincidence-detection nonlinearity, and studied it as a function of the interplay between the encoding and readout timescales. Previous work [32] analyzed this NERM by numerical integration, with $N = 2$ encoding neurons. Here, we extend this work by providing an approximated analytic solution of a more general version of the model, which helps assessing the conditions under which the apparently paradoxical effect of lower encoding but higher transmission of neural information occurs. Previous works have

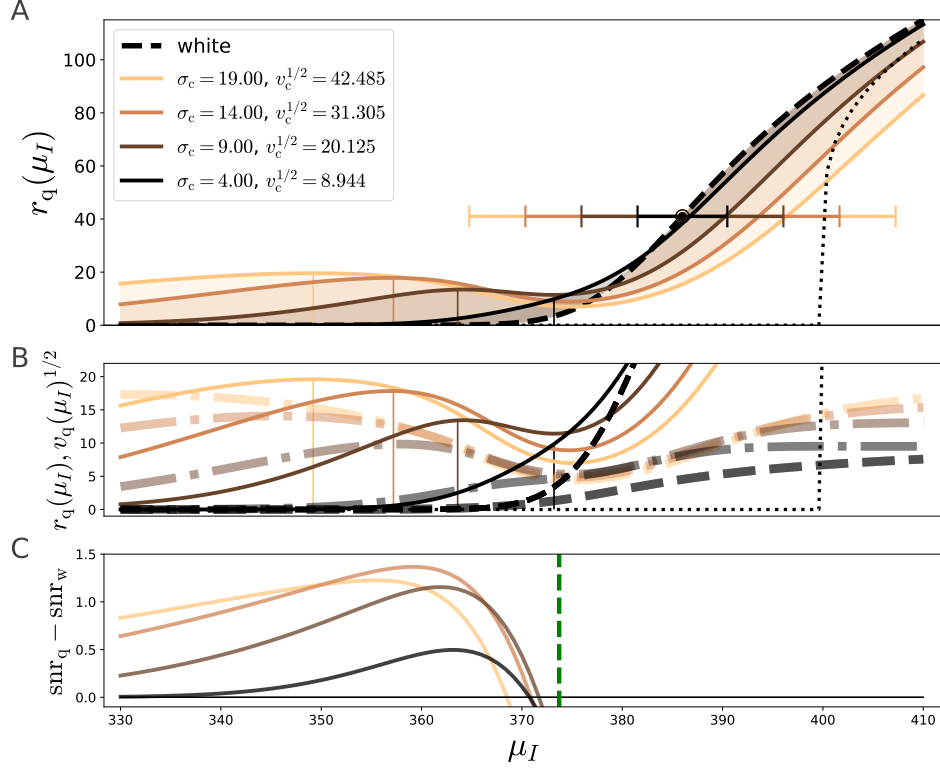


FIG. 9. *Readout rate mean, variance and excess of SNR for negligible values of $r_R^{(-)}$.* (A) Mean firing rate $r_R(\mu_I)$ of the white-noise LIF (dashed line), and the quenched-noise colored-noise LIF $r_q(\mu_I)$ (continuous lines) for various values of σ_c (or $v_c = \sigma_c^2/(\tau_c)$, different curves). For each μ_I , the value of σ_I is set to $\sigma_I = (w\mu_I)^{1/2}$, with $w = 10^{-3}$. As in Fig. 5, the circle and error-bars indicate the inflection point and $v_c^{1/2}$, while the black dotted line indicate the activation function of the deterministic LIF r_0 . (B) A zoom of the panel A, in which we report as well the quenched-noise rate standard deviation, $v_q^{1/2}$ (dashed-dotted lines). The vertical lines indicate the maximum of each $r_q(\mu_I)$ curve. (C) The difference between the SNR $[r_q(\mu_I) - r_q(\mu_I^{(-)})]/[(v_q(\mu_I) + v_q(\mu_I^{(-}))/2]^{1/2}$ (taking a low $\mu_I^{(-)} = 260$, actually equivalent to neglect $r_q^{(-)}$) in the presence of colored noise, minus the white-noise SNR, $[r_w(\mu_I) - r_w(\mu_I^{(-)})]/[(v_w(\mu_I) + v_w(\mu_I^{(-}))/2]^{1/2}$, assuming a Poissonian rate variance, $v_w = r_w$. The vertical dashed line corresponds to our upper bound $\hat{\mu}_I$. Rates and variances are calculated with a $\sigma_I^2 = w\mu_I$ that varies with μ_I for fixed w (see the repository [48]). The rest of the model parameters are: $\tau_c = 0.1$, $\tau_m = 0.0025$, $w = 0.001$, $\mu_I^{(-)} = 260$.

addressed, with analytical approximations, the effect of temporal input correlations on the *mean* output rate of a LIF neuron [10, 16, 17]. Here, we provided alternative, approximated analytical expressions not only for the mean output firing rates (that actually generalize those in [17]), but also for the SNR of information transmission. This constitutes a key extension to evaluate the implications of correlated activity on neural information processing.

We found that the non-linearity of the LIF activation function induces asymmetric fluctuations of the output firing rate, following symmetric *input* fluctuations. The quenched-noise approximation developed here, valid for large or moderate values of $\tau_c \gtrsim \tau_m$, provides the conditions under which these asymmetric fluctuations allow information-limiting noise correlations to enhance the readout SNR. In particular, the following necessary conditions for the mean input current must be satisfied (see Sec. IV B): the readout neuron must operate in a fluctuation-driven regime for low enough $\mu_I^{(+)} < \hat{\mu}_I$, in agreement with the results of [32], with $\hat{\mu}_I(v_c, \tau_m)$ being a decreasing function of v_c and τ_m ; the stimulus-specific difference in *encoding* firing rates $\mu_I^{(+)} - \mu_I^{(-)}$ is high enough (with $\mu_I^{(-)} < \hat{\mu}_I^{(-)}(v_c, \mu_I)$, being $\hat{\mu}_I^{(-)}(v_c, \tau_m)$ a decreasing function of v_c and τ_m). These conditions on the input firing rates confirm previous conclusions that input correlations enhance readout information from a postsynaptic neuron when the readout integration time constant is short enough so that the average excitatory inputs received during an integration window are much smaller than the gap between the spiking threshold and resting potential of the readout neuron, so that output firing is driven by input fluctuations [32].

Beyond the conditions on the encoding firing rates $\mu_I^{(\pm)}$, our analytical solutions reveal necessary conditions on other variables, which were not considered in previous work [32] (see Appendix M). For instance, it reveals conditions on the amplitude of noise correlations, σ_c : this quantity must be large enough for noise correlations to have an impact

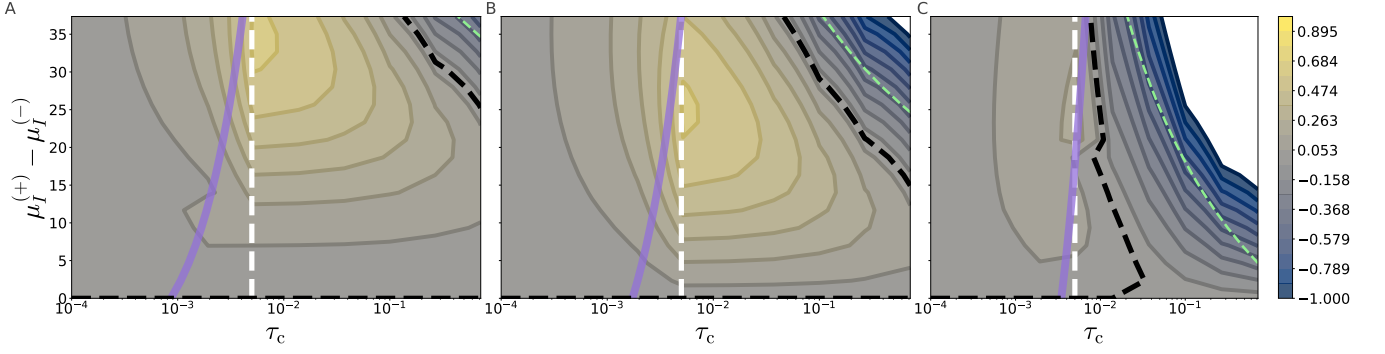


FIG. 10. Contour plot of the excess of SNR (δ_{SNR}) with respect to the absence of noise correlations, versus τ_c and $\Delta\mu_I$. Different panels correspond to different values of $\mu_I^{(-)} = 10, 20, 40$ (A, B, C, respectively). The theoretical SNR has been calculated according to the Poisson-Moreno (low α_M) and quenched-noise (large α_M) approximations. The thick purple line signals the threshold $\alpha_M = 0.75$ that we have used to select the approximation: above and at the left of the purple line, we use Poisson-Moreno, while below and at the right, we use the quenched-noise approximation. The dashed green line indicates the parameter values for which $\mu_I^{(+)} < \hat{\mu}_I$ (a necessary condition for the SNR to increase, assuming a negligible $\mu_I^{(-)}$). The white dashed line indicates τ_m , while the dashed black line indicates the $\delta_{\text{SNR}} = 0$ contour. The rest of the model parameters are: $\alpha_V = 0.9$, $\tau_m = 0.05$, $\sigma_V = 1.104$, $w = 0.45$.

on the SNR numerator Δr_R , but not too large for the SNR denominator $\langle v_R^{(s)} \rangle_{s=\pm}$ to overcome the enhancement in the numerator (Fig. 9 and Sec. IV B). The non-monotonic dependence of the readout SNR on $\sigma_c^2 = 2v_c\tau_c$ and, hence, on τ_c for fixed v_c (Fig. 8) can be clearly understood within the quenched-noise approximation. On the one hand, the larger τ_c , the larger the minimum value of the amplitude σ_c of noise correlations that can elicit a rate enhancement Δr_R (which depends on σ_c only through $v_c = \sigma_c^2/(2\tau_c)$). On the other hand, while Δr_R depends on the stationary variance v_c only, the readout variance v_R increases with *both* v_c and τ_c (and *faster* with v_c , cf. Eq. (13a)). The dependence of the mean readout rate r_R on the stationary variance v_c follows from the quenched-noise approximation *ansatz* itself (Eq. 9). In contrast, the readout rate variance v_R increases with v_c and τ_c , because it is the integration, Eq. (11), of the temporal correlation function (which, in the quenched-noise approximation, decays as an exponential with timescale τ_c and amplitude $Q(v_c)$, see Eqs. (12) and (H4) in Appendix H). As a result, the enhancement of the readout SNR occurs over a wide range of timescales τ_c (or σ_c for fixed v_c), while the SNR decreases at sufficiently large τ_c .

In sum, for the noise correlations to enhance the readout SNR, $\mu_I^{(\pm)}$ should be lower than the inflection point of the white-noise LIF activation function, their difference $\mu_I^{(+)} - \mu_I^{(-)}$ should be large enough, and σ_c should be large enough, but not too large.

The additional necessary conditions derived here have potential implications for the interpretation of biological findings and functions. We have found that information-limiting correlations are useful to enhance information transmission only for intermediate values of the correlation strength σ_c . Across experiments and brain areas, correlation between neurons are reported consistently to be non-zero, but always of small or moderate value [8, 23]. Our result suggests that non-null but moderate values may be useful to design neural codes that trade off effectively the information-limiting and information-enhancing effect of correlations and achieve good levels of information transmission. We have also found that the SNR enhancement may occur for a wide range of time constants of input correlations τ_c , even at values of τ_c much larger than the readout membrane time constant τ_m . This implies that neural circuits may be able to enjoy the benefits of information-encoding-limiting yet information-transmission-enriching correlations even when encoding information with activity correlated over long times. This is important because long encoding timescales are useful to combine temporally separate inputs and accumulate consistently information over time, or to implement or compute a goal-oriented navigation plan [34].

From the methodological point of view, we have proposed a (to our knowledge) novel analytical approximation for the rate mean and variance of the LIF model with white+colored input noise or, equivalently, for the first passage time of a random walker with non-Markovian noise (the *active Brownian particle*, in the terminology of [49, 53]). Despite its conceptual and methodological simplicity, this appears as one of the few existing results regarding the LIF model with temporally and spatially correlated input [22, 49]. The quenched-noise approximation reveals that the colored-noise LIF neuron exhibits a higher-curvature activation function with respect to the white-noise LIF activation function $r_w(\mu_I)$. Moreover, beyond the effect on the average firing rate, the quenched-noise approximation addresses as well how temporal auto-correlations in the input are transmitted into auto-correlations in the colored-LIF output firing rate and, finally, how such auto-correlations shape the rate variance below or above Poissonian fluctuations

$$v_R = r_R/T_c.$$

Our work has considered a single readout neuron. While this simplification is useful to understand in detail the role of neural non-linearities in the transmission of information from temporally correlated inputs, information transmission in the brain happens from input to output populations. Other work [39] has considered the conditions for effective transmission of information between neural populations, although considering only time-averaged spike count responses and neglecting the temporal aspects of correlated activity and neural post-synaptic integration that we considered here. Extending this and previous works will be important to merge the principles of population readout with those of time-correlation and time-integration, to understand how the spatio-temporal structure of neural activity shapes information transmission.

A simplification of our work, shared by other previous attempts to characterize analytically how input correlations change the output firing characteristics of a LIF neuron [17, 46], is that all steps of post-synaptic time integration have been summarized through the membrane potential time constant. We considered synapses having instantaneous dynamics, neglecting both their finite rise time and decay time constants, and we neglected the timescales of dendritic integration [54, 55]. Although our simple model still allows to study effectively some of the consequences of lengthening or shortening of integration time constants by non-membrane contributions (for example, the effect of slower synaptic decay time constants could be recapitulated by increasing the membrane time constant), these simplifications prevent us to study the effect of the interplay between membrane, synaptic and dendritic integration in shaping the input-output information of a neuron [40]. Studying these issues is beyond the scope of the present study and the reach of analytical calculations, and is left for further work.

ACKNOWLEDGEMENTS

We acknowledge Sandro Azaele for pointing out references [56–59]. M. I. is supported by: the European Union -Horizon 2020 Program under the scheme INFRAIA-01-2018-2019 –Integrating Activities for Advanced Communities, Grant Agreement n.871042, “SoBigData++: European Integrated Infrastructure for Social Mining and Big Data Analytics” (<http://www.sobigdata.eu>); by the European Union - NextGenerationEU - National Recovery and Resilience Plan (Piano Nazionale di Ripresa e Resilienza, PNRR), project ‘SoBigData.it - Strengthening the Italian RI for Social Mining and Big Data Analytics’ - Grant IR0000013 (n. 3264, 28/12/2021) (<https://pnrr.sobigdata.it/>); by the Spanish Ministry and Agencia Estatal de Investigación (AEI) through Project I+D+i Ref. No. PID2020-113681GB-I00, financed by MICIN/AEI/10.13039/501100011033 and FEDER, “A way to make Europe”.

Appendix A: Symbols and acronyms and terms used in the article

1. Stationary and count variances

We here explain the *count* (σ^2) vs *stationary* (v) *variance* terminology that we employ in the article. Let $y(t)$ be an Ornstein-Uhlenbeck process, obeying the Langevin equation: $\tau dy = -dt y + \sigma dW$, where dW is a Wiener process. Then [43, 44], the stationary distribution of $P(y)$ has variance equal to $\langle y^2 \rangle - \langle y \rangle^2 = v = \sigma^2/(2\tau)$, and temporal correlation function $c(t) := \langle y(t')y(t+t') \rangle = v \exp(-|t|/\tau)$, where $\langle \cdot \rangle$ is the expectation value with respect to realisations of dW . If $y(t)$ represents the rate of an inhomogeneous Poisson process, the variance of the number of spikes $\text{Var}(\text{rate})$ in a time interval of length T is $\text{Var}(\text{rate}) = \frac{2}{T^2} \int_0^T dt' (T-t')c(t')$. The rate variance in an interval of length $T \gg \tau$ is, hence, $\text{Var}(\text{rate}) = 2\tau v/T = \sigma^2/T$. Hence, v is the *stationary variance of the rate*, while σ^2 is the *variance of the spike count in the unit time interval*.

2. Table of symbols and acronyms

See the acronyms and main symbols used in the article in Tables I and II, respectively.

TABLE I. **Acronyms used in the article.**

acronym	definition
NERM	neural encoding-readout model
SNR	signal-to-noise ratio
NIS	number of integration steps
LIF	leaky integrate-and-fire
ISI	inter-spike interval

Appendix B: The diffusion approximation for the encoding signal

1. Single, inhomogeneous Poisson process with Ornstein-Uhlenbeck rate

We consider an inhomogeneous Poisson process whose rate is $r(t) = \mu + \chi(t)$. The fluctuations around its average are such that $\langle \chi(t) \rangle_\chi = 0$, and $\langle \chi(t)\chi(t') \rangle_\chi$ is a given function of $|t-t'|$, and where $\langle \cdot \rangle_\chi$ is the average over realisations of the noise χ . Let $\rho(t) = \sum_k \delta(t-t_k)$ be the density of spikes of such process, where t_k is the k -th spike. In other words, $\rho(t) = \dot{n}(t)$ where $n(t)$ is the number of spikes $t_k < t$ in a single realisation (conditioned to a fixed realisation of r), and the dot stands for the temporal derivative. We are interested in the two-time correlation function, or the covariance

$$\text{Cov}(\rho(t), \rho(t')) = \langle \rho(t)\rho(t') \rangle - \langle \rho(t) \rangle \langle \rho(t') \rangle \quad (\text{B1})$$

Importantly, the expected value $\langle \cdot \rangle := \langle \langle \cdot \rangle_P \rangle_\chi$ is the annealed average over both sources of stochasticity (over the Poisson spikes given $r(t)$, $\langle \cdot \rangle_P$, and over the realisations of $r(t)$, $\langle \cdot \rangle_\chi$). Let us observe that the variable $n(t+\delta) - n(t)$ is, for a fixed realisation of $r(t)$, and using the definition of inhomogeneous Poisson process, a stochastic variable with average and variance equal to $R(t+\delta) - R(t)$, where R is the primitive of r . To first order in δ , such single realisations of $n(t+\delta) - n(t)$ may be written as:

$$n(t+\delta) - n(t) \simeq \delta r(t) + r(t)^{1/2}(W_{t+\delta} - W_t) \quad (\text{B2})$$

where $W_{t+\delta}, W_t$ are random numbers such that the variance of $W_{t+\delta} - W_t$ is δ . Now, for sufficiently large $\delta r(t)$, the variable $n(t+\delta) - n(t)$ can be taken as normally distributed, and W_t is a Wiener process, since $W_{t+\delta} - W_t \sim \mathcal{N}(0, \delta)$. In this case, dividing Eq. (B2) by δ and taking the $\delta \rightarrow 0$ limit one gets, formally,

$$\rho(t) = r(t) + r(t)^{1/2}\eta(t) \quad (\text{B3})$$

where $\langle \eta(t)\eta(t') \rangle_\eta = \delta(t-t')$ is a white noise (and we now write $\langle \cdot \rangle_P$ as $\langle \cdot \rangle_\eta$). Equation (B3) is the so called *diffusion approximation* to the Poisson process.

In the diffusion approximation (Eq. B3), it is immediate to see, first, that $\langle \rho(t) \rangle_{\eta, \chi} = \langle r(t) \rangle_\chi = \mu$. It is also immediate to compute the temporal covariance, or time-correlation function of ρ 's. Using Eq. (B3) and the correlation functions of the noises χ, η :

$$\text{Cov}(\rho(t), \rho(t')) = \left\langle \langle \rho(t)\rho(t') \rangle_\eta \right\rangle_\chi - \mu^2 = \quad (\text{B4})$$

$$= \langle \chi(t)\chi(t') \rangle_\chi + \delta(t-t') \left\langle r^{1/2}(t)r^{1/2}(t') \right\rangle_\chi = \quad (\text{B5})$$

$$= \langle \chi(t)\chi(t') \rangle_\chi + \delta(t-t') \langle r(t) \rangle_\chi = \quad (\text{B6})$$

$$= \langle \chi(t)\chi(t') \rangle_\chi + \mu \delta(t-t'). \quad (\text{B7})$$

2. Many encoding neurons

We now consider a multivariate Poisson process whose N -dimensional vector of rates $\mathbf{x}(t) = \boldsymbol{\mu} + \boldsymbol{\chi}(t)$ whose fluctuations around its mean $\boldsymbol{\mu}$ satisfy the Ornstein-Uhlenbeck process: $\dot{\boldsymbol{\chi}}(t) = -\boldsymbol{\chi}(t)/\tau_c + (2C/\tau_c)^{1/2} \cdot \boldsymbol{\eta}(t)$, where $^{1/2}$ is the matrix square root, and where C is a covariance matrix. Indeed, the stationary distribution for the solutions $\boldsymbol{\chi}$ of this Ornstein-Uhlenbeck process is a multivariate Gaussian with null mean and covariance equal to C . We define as well the Pearson correlation matrix \bar{C} as: $\bar{C}_{ij} = C_{ij}(v_i v_j)^{-1/2}$, where the $v_i := C_{ii}$'s are the stationary variances of the $\chi_i(t)$'s. Finally, we define the spike count variance of the j -th neuron, $\sigma_j^2 := 2\tau_c v_j$. Following the same reasoning lines of the previous subsection, we learn that, if $\rho_i(t)$ is the firing rate of the i -th Poisson process, it is:

$$\langle \rho_i(t) \rangle = \mu_i \quad (\text{B8})$$

$$\langle \rho_i(t)\rho_j(t') \rangle = \mu_i \delta_{ij} \delta(t-t') + (v_i v_j)^{1/2} \bar{C}_{ij} e^{-|t-t'|/\tau_c}. \quad (\text{B9})$$

Now, if $I(t) = \mathbf{w}^\dagger \cdot \boldsymbol{\rho}(t)$ is the density of spikes of the N processes, weighted by a vector of synaptic weights \mathbf{w} , the covariance $\text{Cov}(I(t), I(t')) = \langle I(t)I(t') \rangle - \langle I(t) \rangle \langle I(t') \rangle$

$$\langle I(t) \rangle = \mu_I \quad (\text{B10a})$$

$$\text{Cov}(I(t), I(t')) = \sigma_I^2 \delta(t-t') + v_c e^{-|t-t'|/\tau_c} \quad (\text{B10b})$$

$$(\text{B10c})$$

where

$$\mu_I = \mathbf{w}^\dagger \cdot \boldsymbol{\mu} \quad (\text{B11a})$$

$$\sigma_I^2 = \sum_{j=1}^N w_j^2 \mu_j \quad (\text{B11b})$$

$$v_c = \frac{\sigma_c^2}{2\tau_c} \quad (\text{B11c})$$

$$\sigma_c^2 = \mathbf{w}^\dagger \cdot C \cdot \mathbf{w}. \quad (\text{B11d})$$

3. The Valente et al 2021 model

The NERM analyzed in this article is actually the generalization, for an arbitrary number of encoding neurons N , of the encoding-and-readout model originally defined in section “A model of enhanced-by-consistency information transmission” in [32]). In reference [32] the encoding neurons are represented by inhomogeneous Poisson processes whose firing rate behaves, given the binary stimulus $s = \pm 1$ as:

$$r_i^{(s)}(t) = \mu_i^{(s)} + \sigma_{V_i} \left(\alpha_V \xi_C(t) + (1 - \alpha_V^2)^{1/2} \xi_i(t) \right) \quad (\text{B12})$$

where $\mu_i^{(s)}$ is the tuning curve and α_V is a real number in $[0, 1]$ modulating the fraction of shared and private noise (in such a way that $\langle \xi_i(t) \xi_j(t' + t) \rangle = \delta_{ij} (2\tau_c)^{-1} \exp(-|t|/\tau_c)$, $\langle \xi_C(t) \xi_C(t' + t) \rangle = (2\tau_c)^{-1} \exp(-|t|/\tau_c)$, $\langle \xi_i(t) \xi_C(t' + t) \rangle = 0$). In this way, the noise variance of the i -th encoding neuron is independent of α_V and equal to $v_{V_i} = \sigma_{V_i}^2 / (2\tau_c)$. The spike rate standard deviation σ_{V_i} is set to be proportional to the difference of the tuning curves $\Delta_{\mu_i} = \mu_i^{(+)} - \mu_i^{(-)}$:

$$\sigma_{V_i} = \nu_V \Delta_{\mu_i} \quad (\text{B13})$$

$$\Delta_{\mu_i} := \mu_i^{(+)} - \mu_i^{(-)} > 0 \quad (\text{B14})$$

and $\nu_V \geq 0$ is a positive noise-to-signal ratio. Taking the noise amplitude σ_V proportional to Δ_{μ_i} , one ensures that for any $\alpha_V > 0$ the noise correlations are information-limiting.

We make notice that Valente et al model is of the form as in the previous subsection, with:

$$\sigma_i = \sigma_{V_i}^2 = \nu_V^2 \Delta_{\mu_i}^2 \quad (\text{B15})$$

$$\bar{C}_{ij} = \alpha_V^2 \quad i \neq j. \quad (\text{B16})$$

If we now suppose that all encoding neurons have equal tuning curves increments, $\Delta_{\mu_m} = \Delta_{\mu}$, and that the vector \mathbf{w} has constant components $w_j = w$, we obtain that the current encoding $I(t)$ satisfies Eq. (B10) with (see (B11)):

$$\mu_I^{(s)} = w N \bar{\mu}^{(s)} \quad (\text{B17})$$

$$\left(\sigma_I^{(s)} \right)^2 = N w^2 \bar{\mu}^{(s)} \quad (\text{B18})$$

$$\sigma_c^2 = 2\tau_c v w^2 N \sigma_V^2 (1 + (N - 1)\alpha_V^2) \quad (\text{B19})$$

where $\bar{\mu}^{(s)}$ is the average of the encoding neuron tuning curves. From these last equations we see that the signal/noise ratio of the input current $\text{snr} = \Delta_{\mu_I} / (\sigma_c^2 + \sigma_I^2)^{1/2}$ monotonically decreases with α_V . Eq. (B10) has the equivalent form:

$$I(t) = \mu_I + \sigma_I \eta(t) + \sigma_c \xi(t) \quad (\text{B20})$$

$$\dot{\xi}(t) = -\xi(t)/\tau_c + \frac{1}{\tau_c} \eta'(t) \quad (\text{B21})$$

(we omit the μ_I - and σ_I -dependence on s), where η, η' are two different continuous time white noises, and $\xi(t)$ is an Ornstein-Uhlenbeck process with timescale τ_c .

4. A difference between the present notations and that of Valente et al

Please, mind the notation difference between [32] and the present article: there, it is assumed that $\text{Cov} \left(x_i^{(s)}(t), x_j^{(s)}(t) \right) = \sigma^2 \tau_c \exp(-|t - t'|/\tau_c)$, so that their parameter σ^2 has a different dependence on τ_c than our $\sigma_{V_i}^2$'s (and than our v_{V_i} 's). Indeed, in their work, the instantaneous Poisson rate $r(u)$ is converted into a time-correlated Poisson rate $r(t; \tau_c)$ in the following way (mind the misprint in their low-pass filter, equation 19):

$$r(t, \tau_c) = \int_0^t du e^{-(t-u)} r(u) \quad (\text{B22})$$

so that $\langle (r(t; \tau_c) - \mu)(r(t'; \tau_c) - \mu) \rangle = \sigma^2 \tau_c \exp(-|t - t'|/\tau_c)$.

Appendix C: Numerical methods

1. Numerical integration of the stochastic differential equation for the readout neuron membrane potential

In the main text, we have presented a stochastic-processes theory of the Valente et al model of coincidence-detection defined in section II. The diffusion approximation (see III A) allows us to treat the membrane potential of the readout LIF neuron as the solution of a stochastic differential equation. In the article, we compare the approximated analytical solutions to such equations, with numerical simulations, that help us to asses the approximations' validity limit. We have, in particular, and as in references [17, 19], numerically solved Eqs. (5) using the Euler-Maruyama method [60, 61], completed with a numerical protocol (see below) that corrects the bias induced by the finiteness of the Number of Integration Steps (NIS) per unit time, n_{is} .

In brief, our numerical estimation for the rate mean and variance, r_R, v_R respectively, are performed as follows. First, we employ the Euler-Maruyama method with $T_c n_{\text{is}}$ integration steps to numerically integrate Eqs. (5) with the desired set of parameters $\mu_I, \sigma_I, \sigma_c, \tau_c, \tau_m$ in a time interval of length T_c . We perform a number of n_{tr} different realisations of such integration, differing in the independent random samples of the white noises η, η' , and in the initial conditions for $\xi(0), v(0)$ (that can either be independently sampled from their stationary distributions, or chosen, as for our numerical results, to coincide with those of the previous realisation in the last instant value). For each realisation, we store the corresponding sequence of deadout neuron spike times \vec{t} . Afterwards, we compute the across-trials average and variance of the rate $n_R(T_c)/T_c$, where $n_R(T_c) = \text{len}(\vec{t})$ in single realisations, and where $T_c = 20$. These are, respectively, our finite- n_{is} estimations for the rate mean and variance, \tilde{r}_R, \tilde{v}_R (circles and squares in Figs. 4,7,8-A,8-B,8-C). Importantly, and as already specified in the main article text, *all the rate variance estimations that we report are rate variances per unit time: $v_R T_c$* . Indeed, both the singular and the regular part of the temporal correlation function C induce rate variances that decreases as $1/T_c$: to eliminate this dependency, we report the variance *in intervals of unit length*. Consequently, the SNR analysed in Secs. IV A, IV B is the SNR *per unit time window*, or: $T_c^{-1/2} \times \text{SNR}$.

2. Error estimation of rate mean, variance, and SNR

As said in the main text, the statistical uncertainty (error-bars) of our estimation \tilde{r}_R in Figs. 4,8-A is computed as the standard deviation of the rate $n_R(T_c)/T_c$ across the n_{tr} trials (hence, multiplied by $T_c^{1/2}$). The errors of our estimations of *the rate variance* in Figs. 7,8-B are the confidence intervals of the Chi-squared distribution with $n_{\text{tr}} = 10^3$ degrees of freedom and a probability of $\alpha_\chi = 0.95$. The errors of the SNR in Fig. 8 correspond to the standard deviation across bootstrap realisations of the n_{tr} realisations of spike times –for each of which we compute the SNR (see [48]). Finally, the uncertainties of the NIS-corrected rates (and β_r , see below) are the errors of the regression (see [48] for details).

3. Parameter fixing

We have performed two sets of numerical simulations: the *1st* and the *2nd sets of simulations*. The 1st set of simulations is to assess the numerical dependence of the SNR with $\mu_I, \tau_c, v_c(\alpha_V), n_{\text{is}}$. It is the set that we use to perform the NIS-corrected estimations of the SNR as a function of τ_c and α_V (in Figs. 4-A,6,7,8-A,8-B,8). The 2nd set of simulations is for a fixed value of n_{is} and α_V , and varying μ_I, α_V . We use it to assess the differences between the Moreno et al, and quenched-noise approximations in Fig. 4-A (use use, indeed, a larger value of v_V , to have larger values of $\alpha_M = \sigma_c^2/\sigma_I^2$ given τ_c and, hence, to explore the region in which Moreno solution is expected to be less accurate than the quenched-noise approximation).

In tables III, IV we report the paramter values of each set (please, see [48] as well).

In both sets, given α_V, τ_c and v_V , we consequently initialize v_c through Eq. (7b) and, consequently, $\sigma_c^2 = 2\tau_c v_c$. Analogously, given w and μ_I , we initialize $\sigma_I = (w\mu_I)^{1/2}$. The number of encoding neurons $N = 20$ is fixed for both simulations, and plays the only role of changing the relation between v_c and α_V in Eq. (7b).

Finally, for Figs. 2,3 we have performed shorter, ad-hoc, single-realisation simulations. There, we simulate the encoding spike trains as well, for visualisation purposes only. In Figs. 2,3, we first integrate a solution $\mathbf{x}(t) = (x_1(t), x_2(t))$ of a two-dimensional Ornstein-Uhlenbeck process for the the encoding rate; we therefore generate the encoding spike trains from an inhomogeneous Poisson distribution with corresponding inhomogeneous rate $\mathbf{x}(t)$ (for visualisation only, not to give them as an input to the LIF membrane potential $V(t)$); we finally integrate the LIF

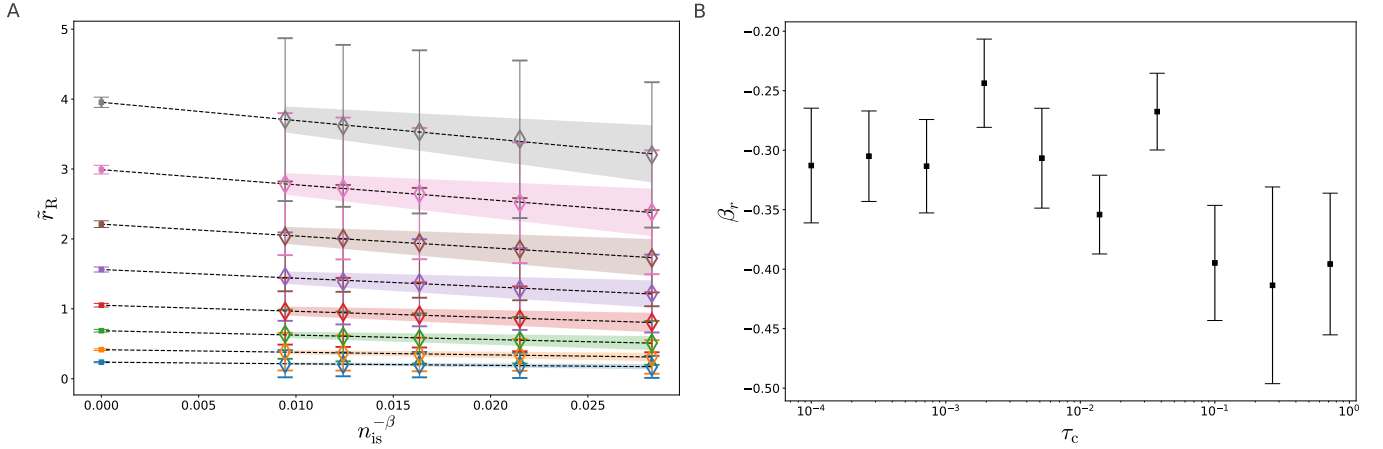


FIG. 11. *Algorithm of finite-NIS-effect reduction.* (A) Numerical estimation of the mean and standard deviation ($\tilde{r}_R, \tilde{v}_R^{1/2}$, diamonds and error-bars, respectively) of the firing rate in single, finite-NIS simulations belonging to the first set (see Sec. C 3), for $\tau_c = 0.7196$ and $\alpha_V = 0.9$, versus $n_{is}^{-\beta}$ (see Table III). Notice that the lowest value of $n_{is} = 2^{14}$ has been omitted, so that $n_{is} = 2^m$ with $m = 15, 16, 17, 18$. Different curves correspond to the different values of μ_I in the 1st simulation set. See Sec. C 2 for details on the estimation of finite-NIS averages and standard deviation $\tilde{r}_R, \tilde{v}_R^{1/2}$. The dotted lines are a linear fit, and the filled area is compressed between the curves $r_\infty(\mu_I) + (b(\mu_I) \pm s_b(\mu_I)) n_{is}^{\beta_r}$ (see Sec. C 4), where $s_b(\mu_I)$ is the standard deviation of the fit result $b(\mu_I)$ for each μ_I (see [48] and [62]). The points at zero abscissa are the extrapolation of the fit results to $n_{is} \rightarrow \infty, r_\infty(\mu_I)$: these are the NIS-corrected values of \tilde{r}_R and its error, in the 1st simulation set (and for this value of τ_c, α_V). (B) The fitted values of β_r for each value of τ_c .

membrane potential $V(t)$ according to Eq. (5), using the rate $\mathbf{x}(t)$ (times a constant, w) at the place of $\mu_I + \sigma_c \xi(t)$ in Eq. (5), consistently with the diffusion approximation.

4. Algorithm of finite-NIS effect reduction

Essentially, our finite-NIS correction algorithm consists in the following simple procedure. Given a simulation for fixed τ_c , we first estimate r_R it for all values of μ_I, n_{is} , obtaining $\tilde{r}_R(\mu_I, n_{is})$ and its statistical uncertainty. Afterwards, we perform a regression of this function as a function of n_{is} , assuming a fitting function $\tilde{r}_R(\mu_I, n_{is}) \simeq r_\infty(\mu_I) + b(\mu_I) n_{is}^{\beta}$, but *forcing the exponent β to assume a common value across the different data $\tilde{r}_R(\mu_I, n_{is})$* , i.e., performing a unique fit for all the μ_I datasets, in which β is μ_I -independent and the rest of the fit parameters r_∞, b are μ_I -dependent. The $n_{is} = \infty$ extrapolated regression parameter $r_\infty(\mu_I)$ is our estimation for the rate mean (for the given τ_c , and the rest of the parameters). Employing this regression protocol, we observe a lower χ^2 variable per degree of freedom, than fixing β , or fitting it for each μ_I separately (please, see the details of the regression protocol in [48]). We repeat this procedure for each τ_c . In Fig. 11-A, we report the fitted values of r_∞ for a given value of τ_c . In Fig. 11-B, we report the fitted values of β vs τ_c . Note the low values of β , that make the raw estimation of the first passage time so slowly dependent on n_{is} and, hence, so inaccurate –and, consequently, the finite-NIS effect mitigation procedure so necessary.

Eventual completions of this work could include a comparison with alternative numerical schemes of integration of stochastic differential equations beyond Euler-Maruyama, as those based on the path integral [58, 59]).

5. Numerical estimation of the temporal distribution function g

In order for the numerical estimation of the temporal distribution function $g(t)$ to be as clear as in Fig. 6, it is necessary to account for the finite- T_c bias of the estimation. In particular, we account for the finite- T_c bias, by computing *the probability couples of spikes to be at a distance $d = |t - t'|$, when the spikes are sampled with uniform probability in the $[0, T]$ time interval*. This cumulative probability can be easily seen to be $\text{Prob}(d < D) = 2D/T - D^2/T^2$, and the probability density is: $\text{prob}(d) = 2/T - 2d/T^2$. Consequently, if we choose arbitrary bins $b_1 < \dots < b_B < T$, it is $\text{Prob}(b_{j-1} < D < b_j) = 2(b_j - b_{j-1})/T - (b_j^2 - b_{j-1}^2)/T^2$.

Our g estimation algorithm works, consequently, as follows: (i) we initialize to zero an array \mathbf{g} of length B . (ii) We put into $\mathbf{g}[i]$ the number of couples of spikes t, t' belonging to the same spike train, across all the n_{tr} spike trains

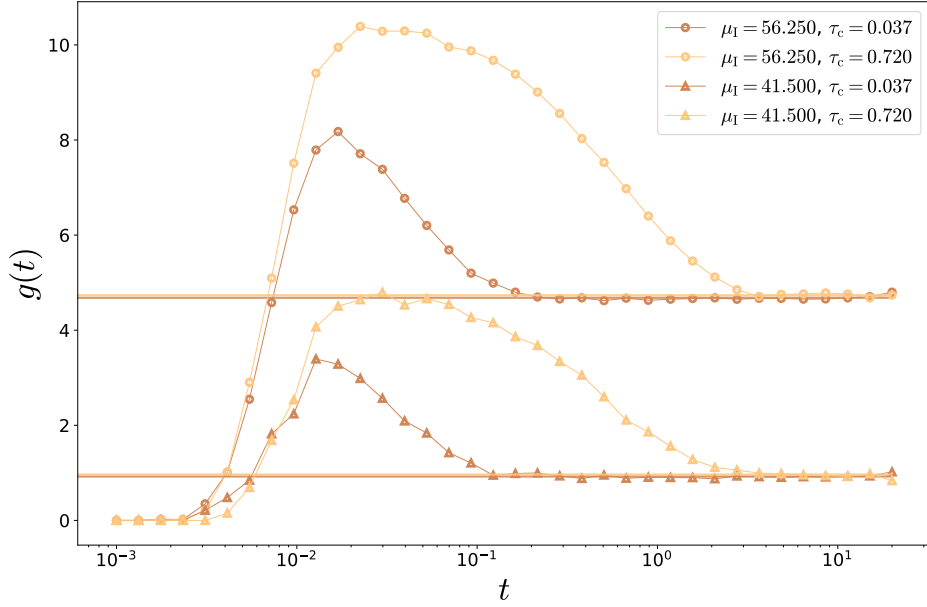


FIG. 12. Numerical estimation of the readout neuron temporal distribution function $g(t)$. Different curves correspond to different values of μ_I and of τ_c (see the figure key) in the 1st simulation set, with $\alpha_V = 0.9$ and $n_{is} = 2^{18}$. The horizontal lines are the NIS-corrected estimations for r_R corresponding to each μ_I, τ_c .

in the simulation, whose distance $d = |t - t'|$ lies in the i -th bin: $b_{i-1} < d \leq b_i$. (iii) $g[i]$ is redefined dividing it by $\text{Prob}(b_{i-1} < D < b_i)$. We expect that, for large enough d , the result is the expected value of the number of couples in an interval T_c (since $\text{Prob}(b_{i-1} < D < b_i) = (\# \text{ couples in the interval } T_c \text{ whose distance lies in the } i\text{-th bin}) / (\# \text{ couples in the interval } T_c)$). (iv) We consequently divide by the expected value of the number of couples of (independent) spikes in T_c , $\langle (n_R - 1)n_R/2 \rangle = (r_R T_c)^2/2$, using our numerical estimation \tilde{r}_R at the place of r_R ; (v) Finally, we multiply this quantity by \tilde{r}_R , to obtain our estimation of g . In this way, the asymptotic value is, as required, r_R . Summarising:

- (i) initialize $g[i] = 0 \forall i = 1, \dots, B$
- (ii) put in $g[j]$ the number of couples of spikes such that $b_{j-1} < |t - t'| \leq b_j, \forall j$ and \forall trials
- (iii) $g[j] /= 2(b_j - b_{j-1})/T_c - (b_j^2 - b_{j-1}^2)/T_c^2, \forall j$
- (iv) $g[j] /= n_{tr}(\tilde{r}_R T_c)^2/2, \forall j$
- (v) $g[j] *= \tilde{r}_R, \forall j$

In Fig. 12 we illustrate the emerging g 's for two values of μ_I and of τ_c . We can see how, indeed, for large enough values of t , $g(t)$ becomes statistically compatible with \tilde{r}_R . This cannot be achieved without correcting for the finite- T_c bias.

Appendix D: Validity range of the approximations

The membrane potential of the LIF readout neuron in the Valente model is described, in the diffusion approximation, by the system of equations (5). Such approximation consists in approximating the statistics of the number of encoding spikes in the time window Δ (sampled from a Poisson distribution with average $\Lambda = \int_{\Delta} dt \mathbf{w} \cdot \boldsymbol{\rho}(t)$) by the statistics of the normal distribution. For the diffusion approximation to be correct, the number of encoding spikes in relevant time windows should be $\gg 1$. In Fig. 13, we show μ_I/r_R , which is the average number of encoding spikes in windows of length equal to the average readout ISI, r_R^{-1} , for all the probed values of μ_I and τ_c , and for both values of α_V . We observe that the average number of encoding spikes in the average readout neuron ISI is, in the worst case, larger than 100, and larger than 1000 in the better case. This is consistent with the diffusion approximation.

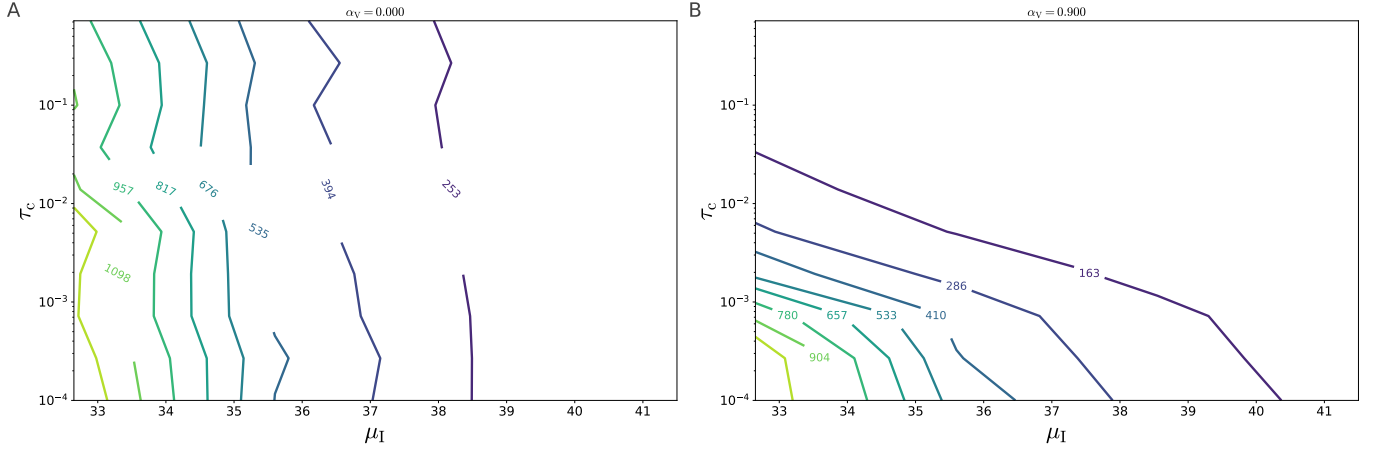


FIG. 13. *Average number of encoding spikes in the average readout neuron ISI, μ_I/r_R , for all the probed values of μ_I and τ_c (in abscissas and ordinates, respectively) in the first simulation set (see Table III). (A) and (B) panels correspond to $\alpha_V = 0, 0.9$, respectively. Given μ_I, τ_c, α_V , we have used the corresponding finite-NIS-corrected estimation of r_R . Colored lines are the iso- μ_I/r_R curves, at equally spaced intervals.*

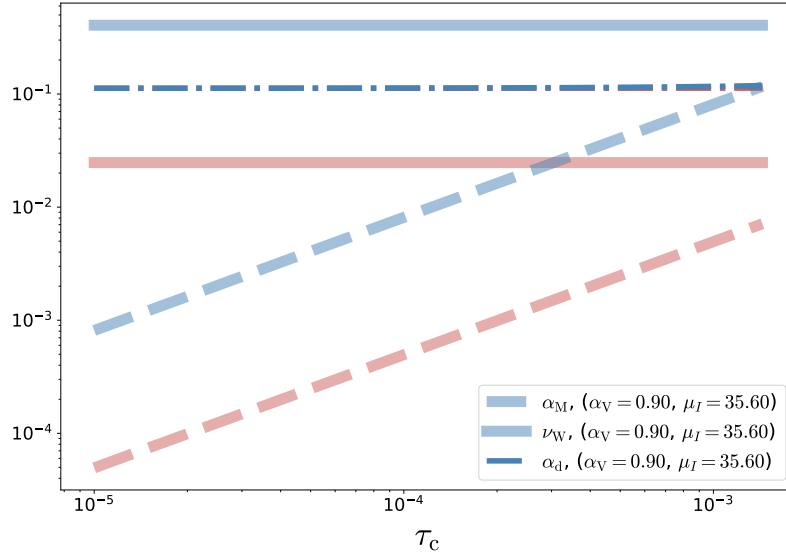


FIG. 14. *The approximation parameters α_M, ν_W and $\alpha_d := (\sigma_c^2 + \sigma_I^2)^{1/2}/\mu_I$, vs τ_c , for $\mu_I = 35.6$ and both values of $\alpha_V = 0, 0.9$.*

For completeness, in Fig. 14 we report the parameters α_M, ν_W and $\alpha_d := (\sigma_c^2 + \sigma_I^2)^{1/2}/\mu_I$ (see Table II), versus τ_c , for two values of $v_V(\alpha_V)$, and for the lowest value of μ_I in our simulations. The fact that the largest value of α_d is at most $\simeq 0.1$, indicates that, again, the parameters of the simulations considered in the article lie in the validity range of the diffusion approximation. An exhaustive assessment of the validity limit of the diffusion approximation is left for future studies.

Analogy with the random walk problem. In the diffusion approximation, valid for $\mu_I \gg (\sigma_I^2 + \sigma_c^2)^{1/2}$ (see [17, 42], the stimulus-readout probability distribution $\text{prob}(\vec{t}|s)$ (on which the SNR depends, through r_R, v_R in Eq. (4)), becomes the distribution of sequences of first passage times of a continuous-time random walker $V(t)$ (see Eq. (5)), with damp $1/\tau_m$, constant drift μ_I , white noise drift $\sigma_I\eta(t)$, colored noise drift $\sigma_c\xi(t)$, and the reset mechanism of the LIF neuron (that conditions the stationary distribution of the ξ 's [18]). The readout neuron Inter-Spike Interval (ISI) time is the first passage time of such a random walker (see [49, 53], and references therein).

Appendix E: Quenched-noise approximation for the LIF neuron firing rate mean

1. The Moreno et al solution

As said in the main text, Moreno et al have shown in [17] that, in the $\tau_c \gg \tau_m$ limit on which we focus, the average firing rate of the coloured-noise LIF model r_R may be approximated, *to first order in τ_m/τ_c , and under the further approximations* of small $\alpha_M = \sigma_c^2/\sigma_I^2$ and small $\mu_I/(\sigma_I^2 + \sigma_c^2)^{1/2}$ (needed for the diffusion approximation), as:

$$r_R(\mu_I) \simeq r_w(\mu_I) \left[1 + \frac{r_w(\mu_I)\tau_m^2\alpha_M}{\tau_c} \left(\tau_m r_w(\mu_I) [R(\Theta_0) - R(H_0)]^2 - \frac{\Theta_0 R(\Theta_0) - H_0 R(H_0)}{\sqrt{2}} \right) \right] \quad (\text{E1a})$$

$$\alpha_M := \sigma_c^2/\sigma_I^2 \quad (\text{E1b})$$

where $r_w(\mu_I)$ is the mean firing rate of a LIF model *with white input noise* (or $\sigma_c = 0$), taking the well-known expression due to Siegert [42, 46]:

$$r_w(\mu) = t_w(\mu)^{-1} \quad (\text{E2a})$$

$$t_w(\mu) = \sqrt{\pi}\tau_m \int_{H(\mu)}^{\Theta(\mu)} dt \phi(t) \quad (\text{E2b})$$

and where $\Theta_0 := \Theta(\mu_I)$, $H_0 := H(\mu_I)$, and:

$$\phi(t) := e^{t^2} (1 + \text{erf}(t)), \quad R(x) := (2/\pi)^{1/2} \phi(x) \quad (\text{E3})$$

$$\Theta(\mu) := \frac{1 - \mu\tau_m}{\sigma_I\sqrt{\tau_m}}, \quad H(\mu) := \frac{-\mu\tau_m}{\sigma_I\sqrt{\tau_m}}. \quad (\text{E4})$$

2. Detailed derivation of the mean firing rate in the quenched-noise approximation

The readout firing rate in the quasi-static approximation is:

$$r_q(\mu_I) := \langle r_w(\tilde{\mu}) \rangle_{\mathcal{N}(\tilde{\mu}|\mu_I, v_c)} \quad \text{quenched-noise app.} \quad (\text{E5a})$$

where $r_w(\mu)$ is the Siegert solution in Eq. (E2). This can be expressed as:

$$r_q(\mu_I) = \int d\mu \left[\frac{1}{2\pi v_c} \right]^{1/2} e^{-Mg(\mu)} \quad (\text{E6a})$$

$$M := \tau_c/\tau_m \quad (\text{E6b})$$

$$g(\mu) := \frac{\tau_m(\mu - \mu_I)^2}{\tau_c} - \frac{\tau_m}{\tau_c} \ln r_w(\mu). \quad (\text{E6c})$$

We will now make use of the Laplace approximation for large M around y_0 (where f is an arbitrary function):

$$\int dy e^{-Mf(x)} \simeq e^{-Mf(y_0)} \left[\frac{2\pi}{Mf''(y_0)} \right]^{1/2} e^{\frac{Mf'(y_0)^2}{2f''(y_0)}} \quad (\text{E7})$$

Deriving once and twice the function g , we immediately arrive to the expression:

$$r_q(\mu_I) = r_w(\mu_I) \left[\frac{1}{1 - v_c g_1'(\mu_I)} \right]^{1/2} \exp \left(\frac{v_c}{2} \frac{g_1^2(\mu_I)}{1 - v_c g_1'(\mu_I)} \right) \quad (\text{E8})$$

where the function $g_1(\mu)$ and its derivative $g'_1(\mu)$ depend on the white LIF parameters only:

$$g_1 = \frac{r_w'}{r_w} = -\frac{t_w'}{t_w} \quad (\text{E9})$$

$$g'_1 = -\frac{t_w'' t_w - t_w'^2}{t_w^2} \quad (\text{E10})$$

$$(\text{E11})$$

We report the explicit expressions for the derivatives of the Siegert mean ISI:

$$t_w' = -\frac{\pi^{1/2} \tau_m^{3/2}}{\sigma_I} [\phi(\Theta) - \phi(H)] \quad (\text{E12a})$$

$$t_w'' = \frac{2\pi^{1/2} \tau_m^2}{\sigma_I^2} [\Theta\phi(\Theta) - H\phi(H)] \quad (\text{E12b})$$

where Θ, H denote the functions in Eq. (E4).

Appendix F: Alternative figures for different values of the model parameters

In Fig. 15 we show our numerical and analytical estimations of r_R versus τ_c (constant v_c), for four values of μ_I . The finite-NIS corrected estimate is statistically compatible with the Moreno et al solution for low enough τ_c and for all values of μ_I (except, perhaps, for the largest one $\mu_I = 50.350$). Rather remarkably, for large enough τ_c and *all the probed values of μ_I* , the finite-NIS-corrected estimation \tilde{r}_R is compatible with the quenched-noise approximation. We make notice that, as expected, for low values of $\mu_I = 32.650, 35.600, 44.450$, the Moreno parameter $\alpha_M = \sigma_c^2/(w\mu_I)$ is large for the Moreno approximation to work well and, indeed, only the quenched-noise approximation is compatible with the (NIS-corrected) numerical data (see Appendix D as well). For large enough $\mu_I = 50.350$, α_M is low enough, so that the Moreno solution approaches the quenched-noise solution for r_R , and becomes statistical compatible with the numerical \tilde{r}_R .

In Figs. 16,17 we show our numerical and analytical estimations of $v_R^{1/2}$ versus μ_I (for two values of τ_c) and versus τ_c (for two values of μ_I , with constant v_c), respectively. We there report as well our NIS-corrected estimations for the rate variance. We have not used such estimations, since they present a relatively larger statistical error (than their r_R counterpart). We observe that, as happens for r_R , and rather remarkably, for low and high enough values of τ_c , the finite-NIS-corrected estimations $\tilde{v}_R^{1/2}$ become, respectively, compatible with the Poisson-Moreno and the quenched-noise approximations.

In Fig. 18 we present the equivalents of Fig. 8 for an alternative value of the input averages, $\mu_I^{(\pm)}$. We observe a qualitatively identical behavior.

Finally, in Fig. 19 we present a variant of Fig. 6 for a different value of μ_I .

Appendix G: Analytical expression for the rate variance in the quenched-noise approximation

1. Sketch of the derivation of the temporal distribution function in the quenched-noise approximation

The quenched-noise approximation to g is as follows. Let $n_j(\ell)$ be the number of LIF spikes in the time interval $[t_j, t_{j+1}]$ where $t_j := j\ell$ and j is an integer in $[0, L = \text{int}(T_c/\ell)]$. We define the *discrete-time temporal distribution function* in the quenched-noise approximation, g_q , as:

$$r_q g_q(t_j - t_{j'}) = \frac{1}{\ell^2} \left\langle \langle n_j(\ell) n_{j'}(\ell) \rangle_{\mathbf{n}|\boldsymbol{\mu}} \right\rangle_{\boldsymbol{\mu}} \quad (\text{G1})$$

where the expected values are, respectively: with respect to the white-LIF neuron probability density $\text{prob}(\mathbf{n}|\tilde{\boldsymbol{\mu}})$ of sequences $(n_1(\ell), \dots, n_L(\ell))$ of L spike counts, given the sequence of L average input rates $(\tilde{\mu}_1, \dots, \tilde{\mu}_L)$; and with respect to the probability of sequences of consecutive mean input rates, $\text{prob}(\tilde{\boldsymbol{\mu}})$. We expect g_q in Eq. (G1) to approximate well g in resolution timescales ℓ satisfying $\tau_m \ll \ell \ll \tau_c \ll T_c$.

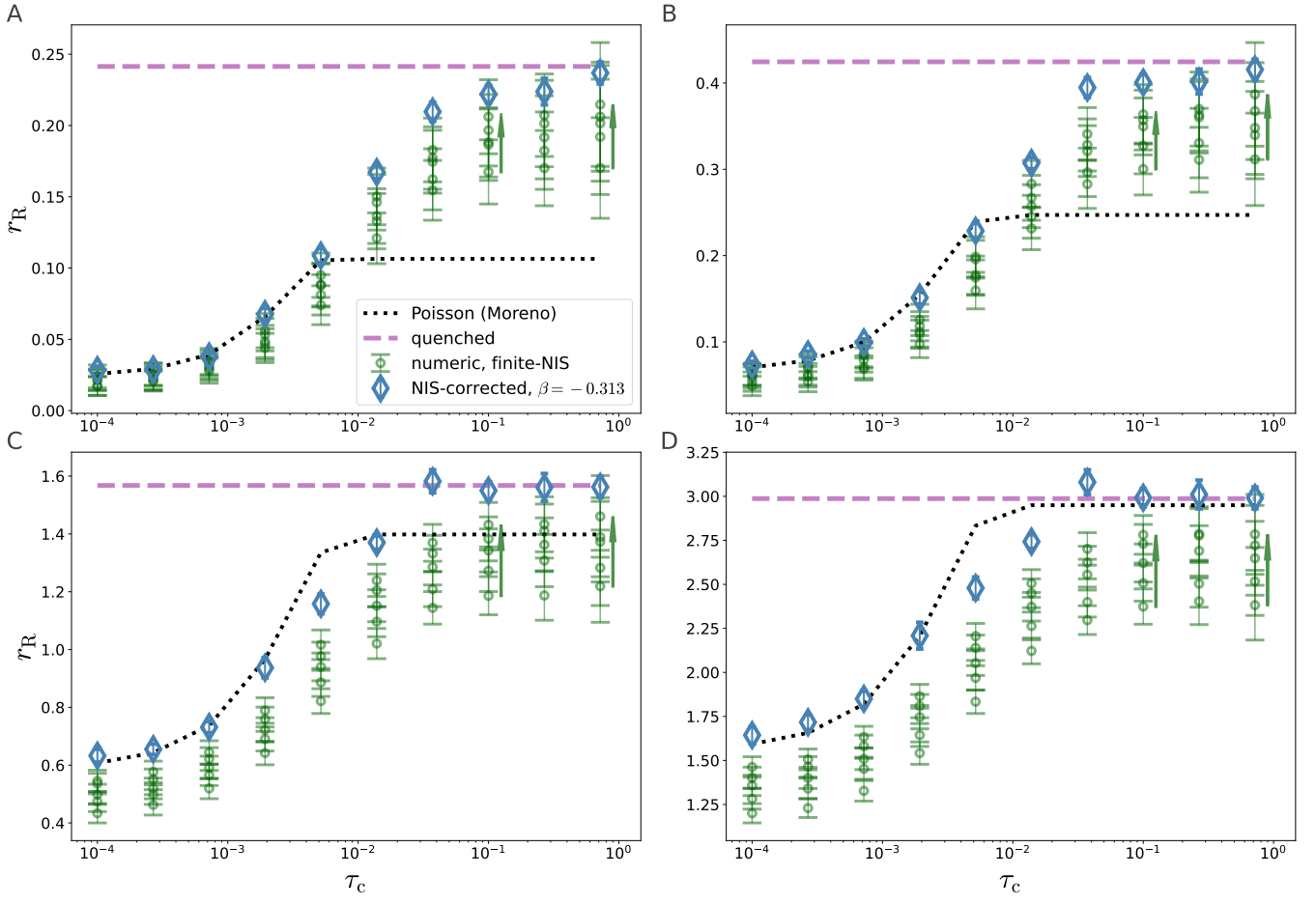


FIG. 15. Mean readout firing rate r_R vs τ_c : comparison between theoretical values and numerical estimations. Panels (A,B,C,D) correspond, respectively, to the different values of $\mu_I = 32.65, 35.0, 44.45, 50.35$. Green points and error-bars are fixed-NIS numerical estimations; blue diamonds and error-bars are the finite-NIS-corrected estimations; the dotted black line is the Moreno extrapolated function in [17], while the pink dashed line is the quenched-noise approximation, Eq. (9).

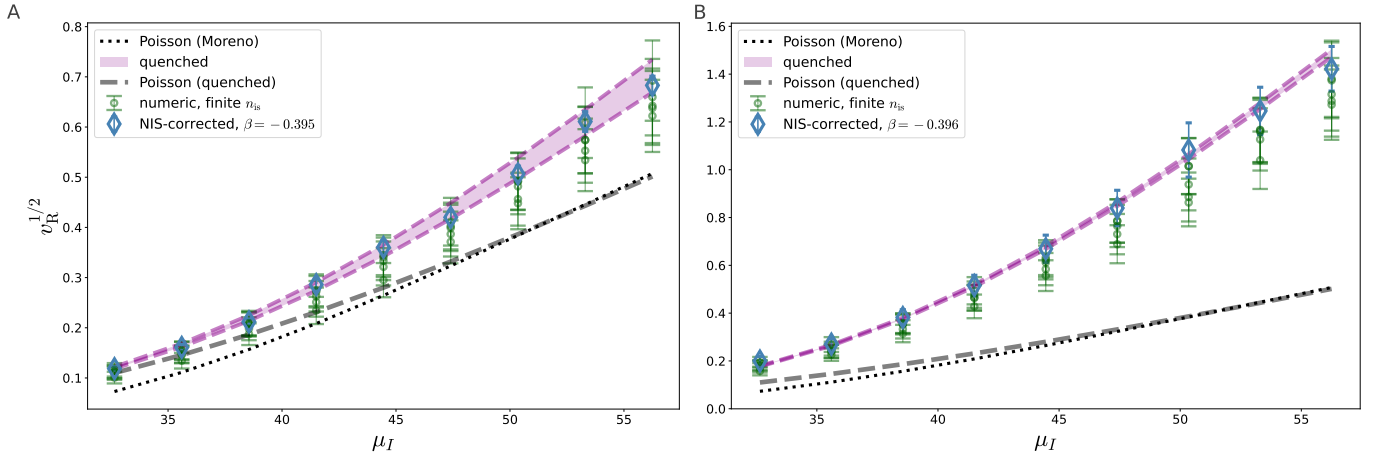


FIG. 16. Standard deviation of the readout firing rate $v_R^{1/2}$ vs μ_I : comparison between theoretical values and numerical estimations. Panels A,B correspond, respectively, to the different values of $\tau_c = 0.1, 0.72$. Green points and error-bars are fixed-NIS numerical estimations; blue diamonds and error-bars are the finite-NIS-corrected estimations; the dotted black line is the Poisson-Moreno approximation $v_R = r_{RM}/T_c$, while the gray dashed line is the Poisson-quenched approximation $v_R = r_{Rq}/T_c$; the pink dashed line fork correspond to the upper and lower-bounds of the quenched-noise approximation, Eq. (13). The rest of the simulation parameters are: $\sigma_c = 30.593$, $\alpha_V = 0.9$, $\tau_m = 0.005$, $w = 0.45$, $v_V = 9.8$.

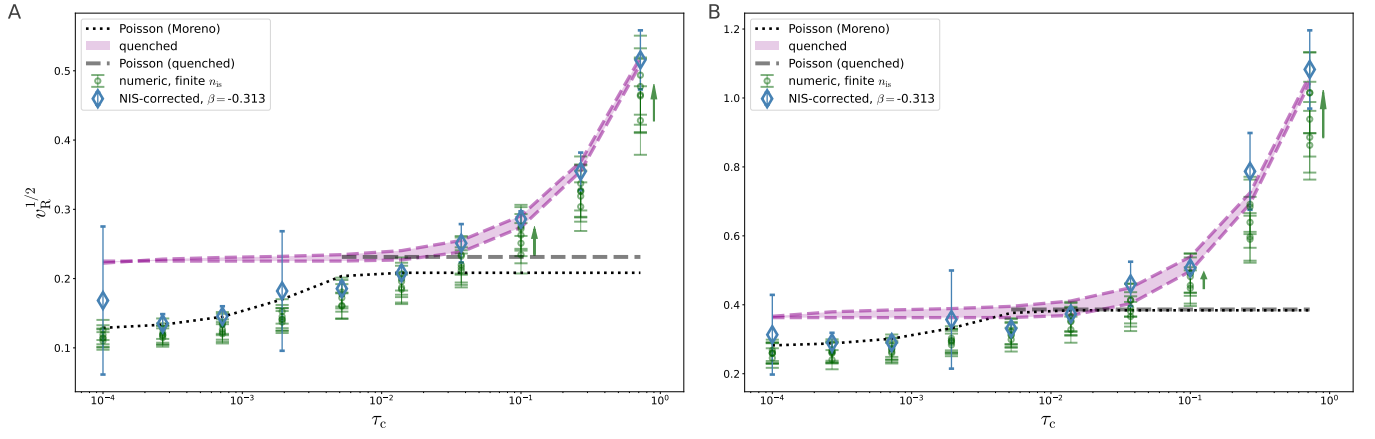


FIG. 17. *Standard deviation of the readout firing rate $v_R^{1/2}$ vs τ_c : comparison between theoretical values and numerical estimations. Panels A,B correspond, respectively, to two different values of $\mu_I = 41.5, 50.35$. The rest of the simulation parameters are: $\sigma_I = 4.760$, $\sigma_c = 0.361$, $\alpha_V = 0.9$, $\tau_m = 0.005$, $w = 0.45$, $vvV = 9.8$.*

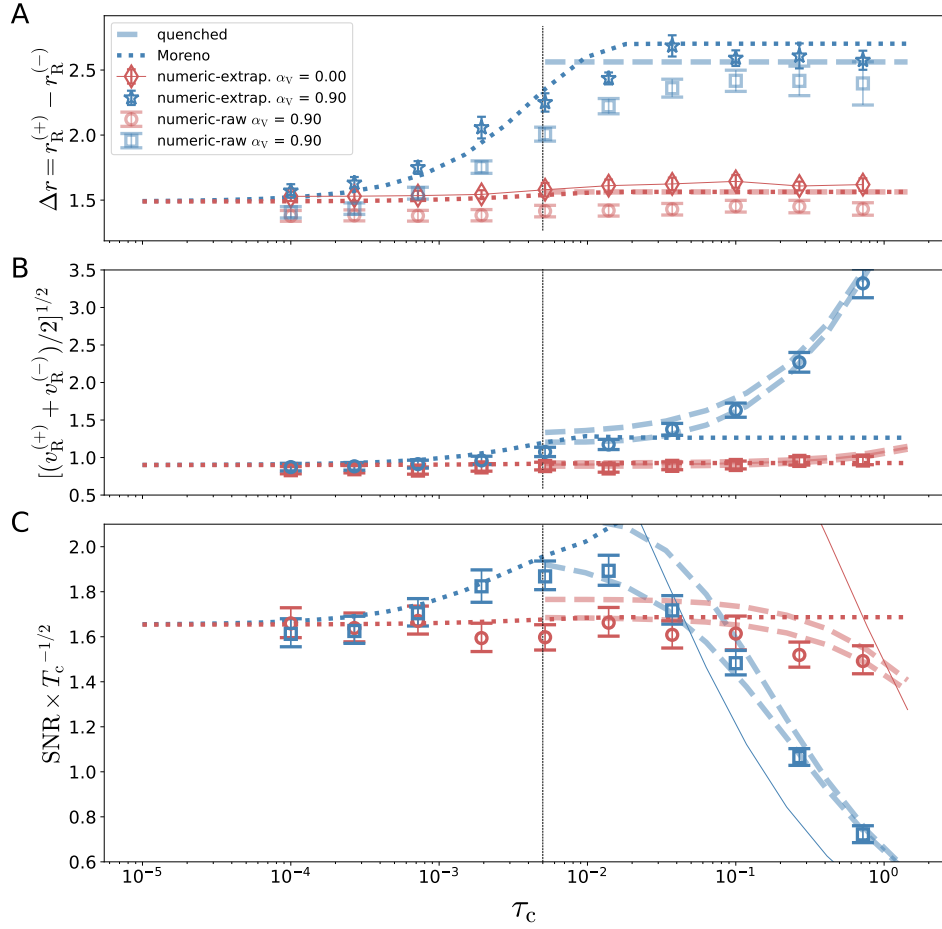


FIG. 18. *Readout SNR in the unit time interval, as in Fig. 8 but for different values of the tuning curves $\mu_I^{(\pm)}$. The simulation parameters are $(\mu_I^{(+)}, \mu_I^{(-)}) = (32.650, 41.500)$, $w = 0.45$, $vvV = 9.8$.*

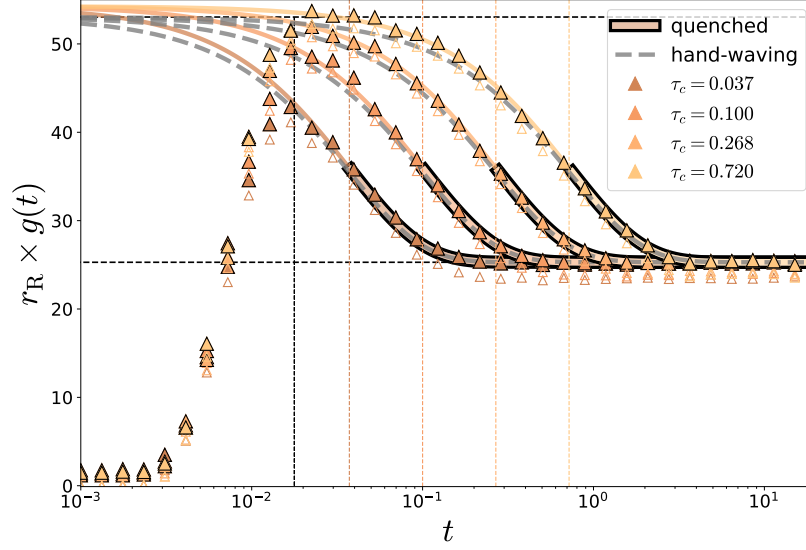


FIG. 19. Temporal distribution function $g(t)$, as in Fig. 6 but for a different value of $\mu_I = 56.25$.

The first hypothesis in our calculation consists in the factorisation of the inner correlation: $\langle n_j n_{j'} \rangle_{\mathbf{n}|\boldsymbol{\mu}} = \langle n_j \rangle_{n_j|\tilde{\mu}_j} \langle n_{j'} \rangle_{n_{j'}|\tilde{\mu}_{j'}}$. Consistently with the quenched-noise approximation, $n_j(\ell)$ can be thought as exhibiting the statistics of the white-LIF neuron, with an input average $\tilde{\mu} \sim \mathcal{N}(\tilde{\mu}; \mu_I, v_c)$. We consequently write $\langle n_j \rangle_{n_j|\tilde{\mu}_j} \ell^{-1} = r_w(\tilde{\mu}_j)$, or: $r_R g_q(t_j - t_{j'}) \simeq \langle r_w(\mu_j) r_w(\mu_{j'}) \rangle_{\boldsymbol{\mu}}$, which in its turn leads to:

$$r_R g_q(t - t') \simeq \int d\mu \int d\mu' r_w(\mu) r_w(\mu') P(\mu, t|\mu', t') P(\mu') \quad (\text{G2})$$

where $t, t' := \ell j, \ell j'$, $P(\cdot) = \mathcal{N}(\cdot; \mu_I, v_c)$ is the stationary distribution of input noises, and $P(\mu, t|\mu', t')$ is the Green's function of an Ornstein-Uhlenbeck process: (mind ξ in Eq. (5)):

$$P(\mu, t|\mu', t') = \mathcal{N}(\mu; \mu_I + \omega\mu', v_c(1 - \omega^2)) \quad (\text{G3})$$

$$\omega := e^{-|t-t'|/\tau_c}. \quad (\text{G4})$$

Both nested integrations, that in $\langle r_w(\mu_t) \rangle_{P(\mu_t|\mu_{t'})}$ (compacting the notation) and, afterwards, that in

$$\left\langle r_w(\mu_{t'}) \langle r_w(\mu_t) \rangle_{P(\mu_t|\mu_{t'})} \right\rangle_{P(\mu_{t'})}, \quad (\text{G5})$$

can be performed in the saddle-point approximation, for large τ_c/τ_m . It is straightforward to arrive to an expression for g_q in the quenched-noise approximation. Interestingly, in the low- and large- $|t - t'|$ limits, the $r_R g_q(t - t')$ take, respectively, the values $\langle r_w^2(\mu) \rangle_{P(\mu)}$ and $\langle r_w(\mu) \rangle_{P(\mu)}^2$ (as expected, since for large $|t - t'|$ we expect μ, μ' to be uncorrelated, and so $r_w(\mu)$ and $r_w(\mu')$). In particular, for large enough $|t - t'|$ (or, more precisely, neglecting terms of order ω^2 in front of first-order terms in ω), we get a simplified expression for g_q :

$$r_R g_q^{(\text{lo-}\omega)}(t - t') \simeq r_q^2 \left(1 + e^{-|t-t'|/\tau_c} Q \right) \quad \text{large } |t - t'|/\tau_c \quad (\text{G6})$$

where Q is a constant in time, depending on the white-LIF properties μ_I, σ_I, τ_m , and on v_c (see the explicit expression in Eq. (G14) below in Sec. G 2).

2. Evaluation of the nested integrals

We want to evaluate the nested integral in Eq. (G2). In the Laplace approximation around $\mu_\omega := \mu_I + \omega\mu'$, and for large $M = \tau_c/\tau_m$ it is:

$$\langle r_w(\mu) \rangle_{P(\mu|\mu')} \simeq e^{-Mf(\mu_\omega)} \left(\frac{2\pi}{Mf''(\mu_\omega)} \right)^{1/2} e^{\frac{Mf'(\mu_\omega)^2}{2f''(\mu_\omega)}} \quad (G7a)$$

$$f(y) := \frac{\tau_m}{\sigma_\omega^2} (y - \mu_\omega)^2 - \frac{\tau_m}{\tau_c} \ln(r_w(y)) \quad (G7b)$$

$$\sigma_\omega := \sigma_c(1 - \omega^2)^{1/2} \quad (G7c)$$

This amounts to:

$$\langle r_w(\mu) \rangle_{P(\mu|\mu')} \simeq r_w(\mu_\omega) \left[\frac{1}{1 - v_\omega g'_1(\mu_\omega)} \right]^{1/2} \exp \left(\frac{v_\omega}{2} \frac{g_1(\mu_\omega)^2}{1 - v_\omega g'_1(\mu_\omega)} \right) \quad (G8)$$

$$v_\omega := \sigma_\omega^2 / 2\tau_c. \quad (G9)$$

We notice that, as required, $\langle r_w(\mu) \rangle_{P(\mu|\mu')}$ coincides with $r_w(\mu')$ for $t = t'$, and with our quenched-noise approximation, $r_R = \langle r_w(\tilde{\mu}) \rangle_{P(\tilde{\mu})}$ for $|t - t'| = \infty$ (or $\omega = 0$). The final step is to perform the integral $\int d\mu' r_w(\mu') \langle r_w(\mu) \rangle_{P(\mu|\mu')}$. It is, in saddle-point approximation around μ_I :

$$r_R g_q(t - t') \simeq \frac{2^{1/2}}{\sigma_\omega} \left(\frac{\tau_c}{\pi \sigma_c^2} \right)^{1/2} \left(\frac{2\pi}{Mh''(\mu_I)} \right)^{1/2} e^{\frac{Mh'^2(\mu_I)}{2h''(\mu_I)}} \quad (G10)$$

$$h(y) := \frac{\tau_m}{\sigma_c^2} (y - \mu_I)^2 - \frac{\tau_m}{2\tau_c^2} \frac{g_1(y_\omega)^2}{f''(y_\omega)} + \frac{\tau_m}{2\tau_c} \ln(f''(y_\omega)) - \frac{\tau_m}{\tau_c} \ln(r_w(y)r_w(y_\omega)) \quad (G11)$$

$$y_\omega := \mu_I + \omega y \quad (G12)$$

where $f''(\mu_\omega) = (2\tau_m/\sigma_\omega^2) - (\tau_m/\tau_c)g'_1(\mu_\omega)$ (see Eq. (G7)).

We will omit the explicit expression of $r_R g(t - t')$, that can nevertheless be straightforwardly unfolded in terms of the derivatives of f and h , that in their turn depend on the first, second and third-order derivatives of r_w . We will actually write an explicit expression for $r_R g(t - t')$ for large values of $|t - t'|/\tau_c$. Neglecting terms of order ω^2 in front of zeroth- and first-order terms in ω , in h'^2 and in h'' , we can evaluate Eq. (G10):

$$r_R g(t - t') \simeq \langle r_w(\mu) \rangle_{P(\mu)}^2 (1 + \omega Q) \quad \text{low } \omega \quad (G13)$$

where:

$$Q := \frac{1}{2} \frac{g_1(\mu_I) [2g_1(\mu_I) + \tau_c^{-1}(F_2 + F_3)]}{v_c^{-1} - g'_1(\mu_I)} \quad (G14)$$

$$F_2 := \left(\frac{g_1^2}{g''} \right)' \Big|_{\mu_I} \quad (G15)$$

$$F_3 := \frac{g_1''}{g''} \Big|_{\mu_I} \quad (G16)$$

The explicit expressions for F_2, F_3 are:

$$F_2 = \left(\frac{g_1^2}{g''} \right)' = \frac{2g_1 g_1' g'' + \frac{1}{\tau_c} g_1^2 g_1''}{g''^2} \quad (\text{G17})$$

$$g'' = \frac{1}{2\sigma_c^2} - \frac{g_1}{\tau_c} \quad (\text{G18})$$

$$g_1' = -\frac{t_w'' t_w - t_w'^2}{t_w^2} \quad (\text{G19})$$

$$g_1'' = 3 \frac{t_w'' t_w'}{t_w^2} - 2 \left(\frac{t_w'}{t_w} \right)^3 - \frac{t_w'''}{t_w} \quad (\text{G20})$$

where t_w', t_w'' and g are in Eq. (E6,E12), and where:

$$t_w'''(y) = 2\sqrt{\pi} \frac{\tau_m^{5/2}}{\sigma_1^3} \left(2\Theta(y)[\Theta(y)\phi(\Theta(y)) + \pi^{1/2}] - 2H(y)[H(y)\phi(H(y)) + \pi^{1/2}] \right). \quad (\text{G21})$$

Appendix H: Hand-waving estimation for the rate variance in the quenched-noise approximation

1. Hand-waving ansatz for the temporal distribution function

We here present a hand-waving argument, consistent with the quenched-noise approximation, that leads to an alternative analytic expression for the rate variance of the LIF model with white+colored noise input. Interestingly, the hand-waving approximation for v_R and g captures relatively well the behaviour of the numeric estimation of these quantities, but *worst than the full quenched-noise calculation in Sec. G, of which the hand-waving approximation is a further simplification* (please, see Figs. 6,7).

The approximation stands on a simple ansatz for the form of the temporal distribution function $g(t) = \langle \varrho(t') \varrho(t' + t) \rangle / r_R$ of the white+colored noise LIF. We suppose it to be of the same functional form $a + b e^{-|t|/\tau_c}$ of the *encoding temporal distribution function* (see Eq. (B10) in Sec. B): $g_{\text{en}}(t) = \langle I(t') I(t' + t) \rangle / \langle I(t') \rangle = (v_c / \mu_I) e^{-|t|/\tau_c} + \mu_I$. The ansatz is:

$$g_{\text{q}}^{(\text{hand})}(t) = \frac{v_{\text{q}}}{r_{\text{q}}} e^{-|t|/\tau_c} + r_{\text{q}}, \quad (\text{H1})$$

where the coefficients $a = r_{\text{q}}$, $b = v_{\text{q}}/r_{\text{q}}$ are fixed so that the ansatz is consistent with the quenched-noise approximation. The emerging stationary variance $C_-(0) = r_{\text{q}} g_{\text{q}}^{(\text{hand})}(0) - r_{\text{q}}^2$ is, indeed, the stationary variance according to the quenched-noise approximation (in analogy with r_{q} in Eq. (E5) in Sec. E):

$$v_{\text{q}}(\mu_I) := \langle r_{\text{w}}(\tilde{\mu})^2 \rangle_{\mathcal{N}(\tilde{\mu}|\mu_I, v_c)} - r_{\text{q}}^2. \quad (\text{H2})$$

A straightforward calculation in the saddle-point approximation, completely analogous to that in Sec. E, leads to:

$$v_{\text{q}}(\mu_I) + r_{\text{q}}^2(\mu_I) = r_{\text{w}}(\mu_I)^2 \left[\frac{1}{1 - 2v_c g_1'(\mu_I)} \right]^{1/2} \exp \left(\frac{2v_c g_1^2(\mu_I)}{1 - 2v_c g_1'(\mu_I)} \right). \quad (\text{H3})$$

We can now compute the $\text{Var}(\text{rate})$ associated to our $g_{\text{q}}^{(\text{hand})}$ in Eq. (H1), using the relation between $\text{Var}(\text{rate})$ and C_- in Eq. (11), and taking r_{q} as the amplitude of the singular part of $C(t) = r_{\text{q}} \delta(t) + C_-(t)$, with $C_-(t) = r_{\text{q}} g_{\text{q}}^{(\text{hand})}(t) - r_{\text{q}}^2$. The result is our hand-waving expression for the rate variance:

$$\text{Var} \left[\frac{n_R(T_c)}{T_c} \right] \simeq \frac{r_{\text{q}}}{T_c} + \frac{2\tau_c}{T_c} v_{\text{q}}. \quad (\text{H4})$$

2. The variance of step-inhomogeneous Poisson processes

We will now see that Eq. (H4) can be found in an alternative, easily interpretable manner. In Eq. (H4), the first term corresponds to the variance of the rate of a *homogeneous Poisson process whose firing rate is equal to the firing rate in the quenched-noise approximation*. The second term in Eq. (H4) accounts for the inhomogeneity of the rate of the Poisson process. Overall, Eq. (H4) corresponds to the variance of an *inhomogeneous Poisson process such that the firing rate is constant in time windows of length $2\tau_c$ and, within each window, it assumes a constant, stochastic value $r_\mu := r_w(\mu)$, where μ is independently sampled from the stationary probability distribution $\mathcal{N}(\mu; \mu_I, v_c)$ in the quenched approximation*.

In other words, our hand-waving approximation to the variance of our white+colored-noise input LIF neuron for $\tau_c \gg \tau_m$ in Eq. H4, can be seen to emerge as well under the following set of assumptions:

1. The rate variance $\text{Var}[n_R(T_c)/T_c]$ of the white-noise LIF neuron with $\sigma_c = 0$ and input mean μ can be well approximated with the variance of a Poisson process with the corresponding firing rate $\text{Var}[n_R(T_c)/T_c] \simeq r_w(\mu)/T_c$. This assumption (also adopted in the above derivation of Eq. (H4)) is approximately satisfied in the parameter region considered in our analyses. Indeed, for null or low enough σ_c , the variance deviations from Poisson are of the same order of the numerical estimation uncertainty of v_R , or lower, see Fig. 7.
2. The dynamics of the input current I can be approximated with a process in which I is constant in time intervals of size $T_s = 2\tau_c$, and independently sampled across different intervals, from its stationary distribution. We assume, in other words, that the encoding current correlation functions can be approximated as: $\text{Cov}(I(t'), I(t' + t)) = v_c \text{Heav}(2\tau_c - t)$, where Heav is the Heaviside function.
3. Within time windows of size as large as $2\tau_c$, the LIF effectively behaves as a white-noise LIF with *constant input current* μ , sampled from its stationary distribution according to the quenched-noise approximation.

Let us derive Eq. (H4) under these assumptions. Let the time interval of length T be divided into M small intervals of length $T_s = T/M$ so that r_μ is constant in such smaller intervals. The number of spikes $n(T)$ is, in the large interval of length T , a stochastic variable that can be expressed as $n(T) = \sum_{m=1}^M n_m(T_s)$, where $n_m(T_s) := n(mT_s) - n((m-1)T_s)$ is the number of spikes in the m -th small interval. Now, let the $n_m(T_s)$'s be independent and identically distributed, and that their average and variance be finite. Then, the Central Limit Theorem wants, for sufficiently large M , the average rate $n(T)/T$ to exhibit mean and variance as follows:

$$\left\langle \frac{n(T)}{M} \right\rangle \simeq \langle n_m(T_s) \rangle \quad (\text{H5})$$

$$\text{Var} \left[\frac{n(T)}{M} \right] \simeq \frac{1}{M} \text{Var} [n_m(T_s)] \quad (\text{H6})$$

where expectation values and variances refer to the annealed probability distributions of both the realisations of the Poisson spikes given r_μ , and of the different instances of r_μ . This is equivalent to suppose that one first samples M independent $\mu \sim \mathcal{N}(\cdot; \mu_I, v_c)$ and, for each of such μ 's, one samples $n_m(T_s) \sim \text{Poisson}(\cdot; T_s r_\mu)$.

The average of the single n_m 's is:

$$\langle n_m(T_s) \rangle = \left\langle \langle n_m(T_s) \rangle_{P|\mu} \right\rangle_\mu = T_s \bar{r} \quad (\text{H7})$$

$$\bar{r} := \langle r_\mu \rangle_\mu \quad (\text{H8})$$

where we have used that the average over the joint probabilities on n_m 's and μ 's is $\langle \cdot \rangle = \left\langle \langle \cdot \rangle_{P|\mu} \right\rangle_\mu$, where $\langle \cdot \rangle_{P|\mu}$ refers to the expectation over the conditional probability $\text{Poisson}(\cdot; T_s r_\mu)$, and $\langle \cdot \rangle_\mu$ the expectation according to $\mathcal{N}(\cdot; \mu_I, v_c)$. In the above online equation, the identity $\langle n_m(T_s) \rangle_{P|\mu} = r_\mu$ is just the equation for the average of $\text{Poisson}(\cdot; T_s r_\mu)$.

The variance of the single n_m 's is:

$$\text{Var} [n_m(T_s)] = \left\langle \left\langle (n_m(T_s) - T_s \bar{r})^2 \right\rangle_{P|\mu} \right\rangle_\mu \quad (\text{H9})$$

where we have used Eq. (H7) $\langle n_m(T_s) \rangle = T_s \bar{r}$. Now, sum and subtract $T_s r_\mu$ within the parentheses, to get:

$$\text{Var}[n_m(T_s)] = \left\langle \left\langle (n_m(T_s) - T_s r_\mu)^2 \right\rangle_{P|\mu} \right\rangle_\mu + T_s^2 \left\langle (\bar{r} - r_\mu)^2 \right\rangle_\mu \quad (\text{H10})$$

where we have used again Eq. (H7). Using the equation for the variance of the Poisson distribution $\left\langle (n_m(T_s) - T_s r_\mu)^2 \right\rangle_{P|\mu} = T_s r_\mu$, we finally get:

$$\text{Var}[n_m(T_s)] = T_s \bar{r} + T_s^2 \text{Var}_\mu[r_\mu]. \quad (\text{H11})$$

Now, we are interested in the variance of the rate $n(T)/T$. It is $\text{Var}[n(T)/T] = (M^2/T^2) \text{Var}[n(T)/M]$ and, using the Central Limit Theorem argument in Eq. (H6):

$$\text{Var}\left[\frac{n(T)}{T}\right] \simeq \frac{\bar{r}}{T} + \frac{T_s}{T} \text{Var}_\mu[r_\mu] \quad (\text{H12})$$

Now, taking $T_s = 2\tau_c$ we get Eq. (H4).

Appendix I: The encoding SNR

In Fig. 8 we compared the readout SNR with the *encoding* SNR, and noticed that the later may become lower than the former. This fact is consistent with the data processing inequality [63], stating that, whenever $X \rightarrow Y \rightarrow Z$ is a Markov chain, or (overloading the symbol P) whenever $P(X, Y, Z) = P(X)P(Y|X)P(Z|Y)$, their mutual information satisfy $I(\hat{X}; \hat{Z}) \leq I(\hat{X}; \hat{Y})$. Let X be the stimulus s , Y be the number of encoding spikes (from any encoding neuron) in the time interval $[0, T_c]$, $n(T_c)$, and Z be the number of readout spikes in $[0, T_c]$, $n_R(T_c)$. First, the quantity that we have chosen to quantify the information carried by X and Y or Z is not the mutual information, but the encoding and readout signal-to-noise ratios (that, indeed, depend on the statistics of $Y|X$ and of $Z|X$, respectively). But, most importantly, the readout variable $Z = n_R(T_c)$ does not depend on the encoding number of spikes only, but on the whole history of encoding density of spikes, $\mathcal{R} = (\rho(t))_{t=0}^{T_c}$. In other words, if as variables X, Y, Z we chose $s, n(T_c), n_R(T_c)$, the data processing inequality does not apply, since $P(Z)$ is not a function of Y only: $p(Z|Y)$ does depend on X . Some information regarding the stimulus is actually encoded in the temporal fluctuations of the current $(\rho(t))_{t=0}^{T_c}$, not only through the number of spikes $n(T_c) = \int_0^{T_c} dt \rho(t)$.

Appendix J: Dependence on τ_c of the colored noise amplitude

We are interested in the dependence of the readout rate mean and variance, $r_R^{(s)}, v_R^{(s)}$, on the encoding and decoding properties in the Valente model. In order to study the dependence on the correlation time τ_c , there are two possibilities (see references in [21]). The first one is to consider that the stationary noise amplitude v_c is constant with respect to τ_c (being $\sigma_c = (2\tau_c v_c)^{1/2}$ consequently a function of τ_c). The second one is taking σ_c^2 constant with respect to τ_c (and, hence, τ_c -dependent stationary noise amplitude $v_c = \sigma_c^2/(2\tau_c)$). The first scenario is suitable to address the $\tau_c \rightarrow \infty$ limit of our problem since, if v_c is constant, the colored noise does have an influence for infinitely large τ_c (indeed, $\text{Cov}(I(t), I(t')) = v_c$, see Eq. (7)), while for $\tau_c \rightarrow 0$ the coloured noise has no influence (indeed, $\text{Cov}(I(t), I(t')) = 0$). Oppositely, the constant- σ_c scenario is the suitable one to consider the $\tau_c \rightarrow 0$ regime of the encoding-readout model, since for $\tau_c \rightarrow 0$ the colored noise term $\sigma_c \xi(t)$ reduces to a delta-correlated noise ($\text{Cov}(I(t)I(t')) = (\sigma_I^2 + \sigma_c^2)\delta(t - t')$, see Eq. (7)), while for infinite τ_c it vanishes.

In this work, we analyze the behavior of the readout neuron SNR, both according to the analytical and numerical solutions of the stochastic differential Eq. (5), for several values of the parameters. For the τ_c -dependency, we consider constant stationary variance v_c , since we are specially interested in the behavior of the SNR in the moderate and large- τ_c regimes. The $\tau_c \rightarrow 0$ limit is less interesting in what, even in the case of constant σ_c , the colored-noise LIF neuron behaves for $\tau_c = 0$ as a white-noise LIF neuron with white noise amplitude equal to $\sigma_I^2 + \sigma_c^2$. In this situation, the readout SNR could increase in the presence of small- τ_c noise correlations, but not if one chooses, as a reference, the white-LIF readout with white-noise amplitude $= \sigma_I^2 + \sigma_c^2$. Oppositely, and as show in this article, for constant

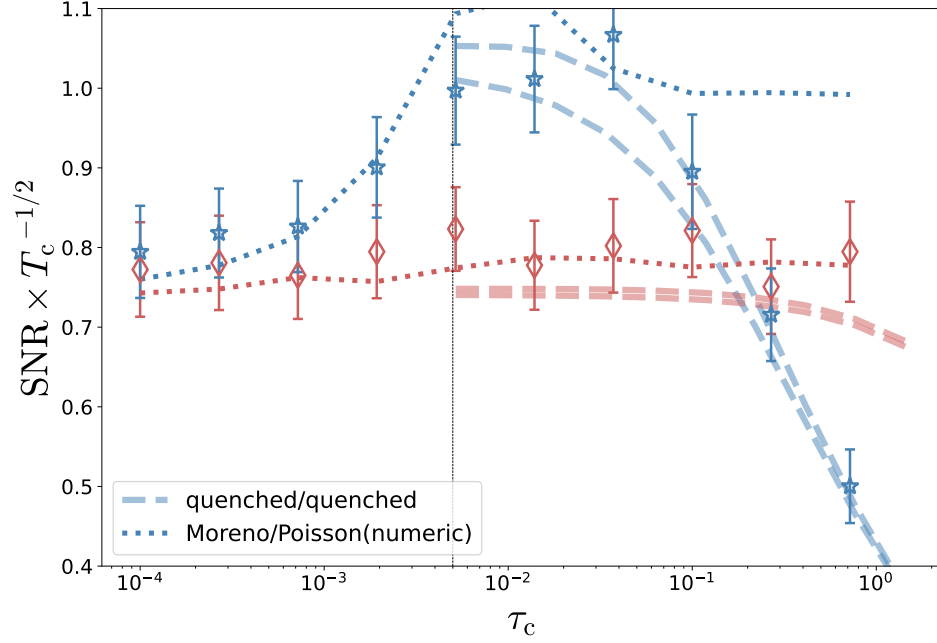


FIG. 20. SNR vs τ_c , as in Fig. 8, but using the NIS-corrected estimator for the numerator, Δr_R .

v_c and large values of τ_c , the behavior of the colored-noise LIF is non-trivially different from that of the white-noise LIF.

We stress that, in any case, the constant v_c choice does not imply loss of generality, as it only determines the value of σ_c that we probe when varying τ_c . Equation (7) tells us that, the larger the value of τ_c , the larger must be σ_c in order for the colored noise term to have a significant impact in $I(t)$, hence in the readout neuron statistics. Taking constant v_c , we automatically accounts for this issue. The constant- σ_c scenario is left to future studies.

Appendix K: Underestimation of the rate variance

As already mentioned, we do not employ, in the main text, the finite-NIS correction algorithm to the variance, since it leads to large errors. Consequently, our estimations for v_R are slightly underestimated. This is, however, not a serious issue since, as we said, the overestimations in the numerator and denominator of the SNR in Fig. 8 partially cancel. In Fig. 20 we report the SNR but, differently from Fig. 8, we use the NIS-corrected estimation for the numerator, Δr_R . In this situation, for our approximations to work well in the $\tau_c \ll \tau_m$ limit, one has to use the Poisson-Moreno approximation, but taking *the numerical estimation for r_R (not the Moreno theoretical one) in the Poisson hypothesis*: $v_R = \tilde{r}_R/T_c$. This works, because the Poisson hypothesis $r_R \simeq \tilde{r}_R/T_c$ still holds for finite n_{is} , when both r_R , v_R are underestimated. We consequently expect that the SNR in Fig. 20 is an overestimation of the SNR (since the numerator is NIS-corrected, while the denominator is underestimated), while the one in Fig. 8 is a more accurate estimation.

Appendix L: SNR versus $\mu_I^{(-)}$

See Figs. 21,22 for an analysis of how the SNR depends on $\mu_I^{(\pm)}$ and on σ_c . The figure illustrates how the behaviour in Fig. 9 (in which $\mu_I^{(-)}$ is so low that $r_R^{(-)}$ is negligible) changes for non-vanishing values of $r_R^{(-)}$.

Appendix M: Theoretical SNR dependence on other variables

For completeness, we report the behavior of the SNR per unit time in as a function of the parameters τ_m , w , α_V , according to our Moreno et al and quenched-noise theories.

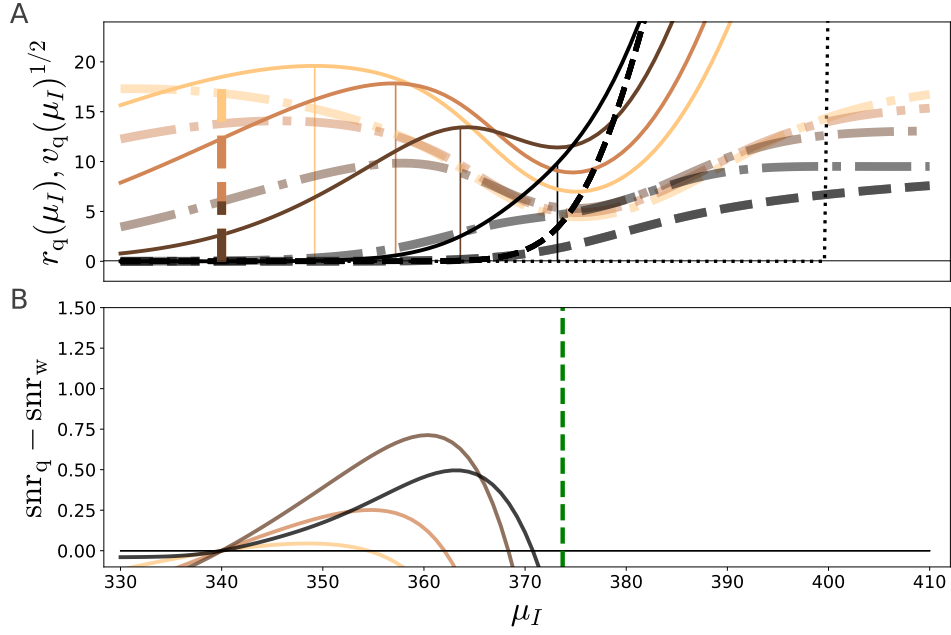


FIG. 21. Readout rate mean, variance, and excess of SNR, as in Fig. 9, but for a higher $\mu_I^{(-)} = 340$ (signaled as a dashed vertical line). The rest of the model parameters are: $\tau_c = 0.1$, $\tau_m = 0.0025$, $w = 0.0010$.

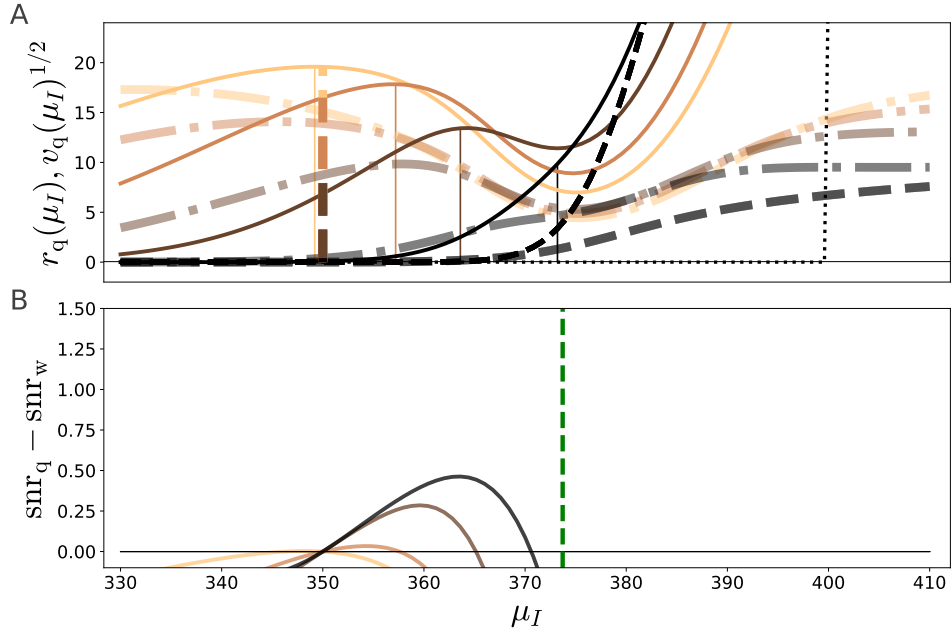


FIG. 22. Readout rate mean, variance, and excess of SNR, as in Fig. 21, but for an even higher $\mu_I^{(-)} = 350$ (signaled as a dashed vertical line).

In Figs. 23,24,25, the SNR has been estimated according to our analytical solutions: for low α_M , we use the Moreno et al solution for Δr_R (interpolated between the $\tau_c \ll \tau_m$ and $\tau_c \gg \tau_m$ solutions, as in [17]), and a Poisson-Moreno hypothesis for the denominator $\langle v_R^{(s)} \rangle_s$ (i.e., supposing $v_R = r_R/T_c$, and the Moreno expression for r_R); for large α_M , we use the quenched-noise approximation for both the numerator and the denominator of the SNR. In practice, whenever α_M is larger than a threshold $\hat{\alpha}_M = 0.75$, we use the quenched-noise approximation. The green dashed line in Figs. 10,23,24,25 signals the $\alpha_M = \hat{\alpha}_M$ transitions in the $(\Delta\mu_I, \tau_c)$ plane. Although the Moreno and quenched-noise approximations are expected to hold only in the $\tau_c \ll \tau_m$ and $\tau_c \gg \tau_m$ limits, respectively, in practice they are relatively congruent around the $\alpha_M = \hat{\alpha}_M$ line for intermediate values of τ_c .

Dependence on τ_m . In Fig. 23 we see how the SNR contour plots change with the value of τ_m . We observe a qualitatively identical effect: reducing τ_m has the effect of shifting the white-noise LIF activation function r_w to the right (mind that r_w depends on μ_I through $\mu_I \tau_m^{1/2}$ in Eq. (E2)), which has a similar effect, qualitatively, as lowering μ_I , and vice-versa.

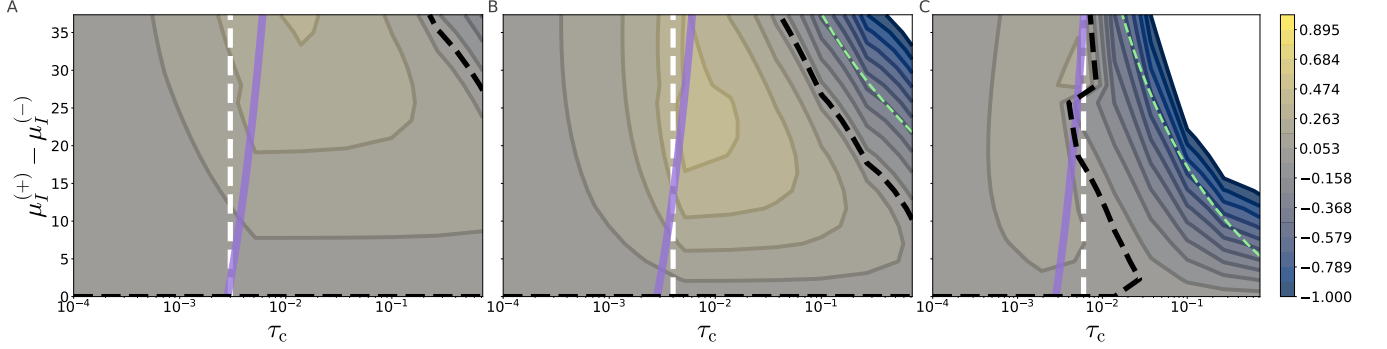


FIG. 23. *Contour plot of the excess of SNR with respect to the absence of noise correlations*, as in Fig. 10, except that panels A,B,C correspond, respectively, to different values of $\tau_m = 0.03, 0.04, 0.06$. The rest of the model parameters are: $\mu_I^{(-)} = 32.65$, $\sigma_V = 1.104$, $\alpha_V = 0.9$, $w = 0.45$.

Dependence on w . In Fig. 24 we see the SNR as a function of w . The dependence on w is qualitatively equal to that on $\mu_I^{(-)}$ in Fig. 23: low w implies a shift of the activation functions to the right (see Fig. 5): for low enough w , reducing w has the same qualitative effect than increasing $\mu^{(+)}$ (panels A,B). Increasing w beyond a certain threshold, $\mu_I^{(+)}$ approaches $\hat{\mu}_I$, and eventually also $\mu_I^{(-)}$ approaches $\hat{\mu}_I^{(-)}$: hence, the SNR decreases everywhere in the $\Delta\mu_I, \tau_c$ plane.

Dependence on α_V . We report the dependence with σ_c (equivalently, α_V) in 25, for $\alpha_V = 0.25, 0.9, 1.5$. The largest probed value of α_V is larger than one. While this is not, in principle, possible according to the definition of encoding noise correlations, in this section it is an effective way of increasing $\sigma_c(\alpha_V) = w\sigma_V[N(1 + (N-1)\alpha_V^2)]^{1/2}$, above the value that it would have for $\alpha_V = 1$ (see Sec. C), and that could correspond to an equivalent increment in N , w or σ_V , keeping $\alpha_V \leq 1$. First, for low enough α_V (panel A), the amplitude of noise correlations is too low to imply a significant increment of SNR. For larger values of α_V , the non-monotonic dependence along both axes that we described in Sec. IV B emerge (panel B). For larger and larger α_V , and for a high enough value of $\mu_I^{(-)}$, near enough $\hat{\mu}_I^{(-)}$, the maximum of the SNR moves to the left, in the x-axis (panels B,C). This means that, at a fixed value of $\mu_I^{(\pm)}$, increasing the value of σ_c may imply a lower $\hat{\mu}_I^{(-)}$ and, consequently, a lower SNR, as we explained in Fig. 21.

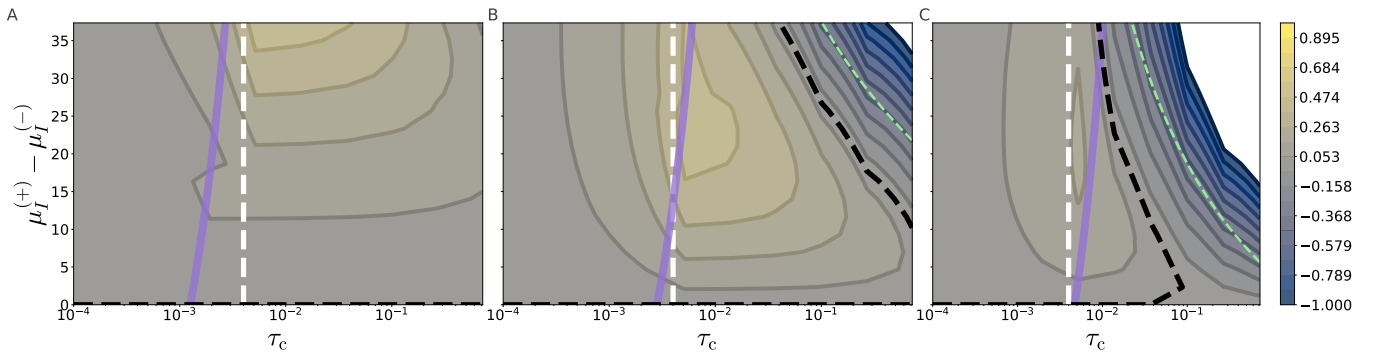


FIG. 24. *Contour plot of the excess of SNR with respect to the absence of noise correlations*, as in Fig. 10, except that panels A,B,C correspond, respectively, to different values of $w = 0.2, 0.45, 0.75$. The rest of the model parameters are: $\mu_I^{(-)} = 32.65$, $\tau_m = 0.04$, $\sigma_V = 1.104$, $\alpha_V = 0.9$.

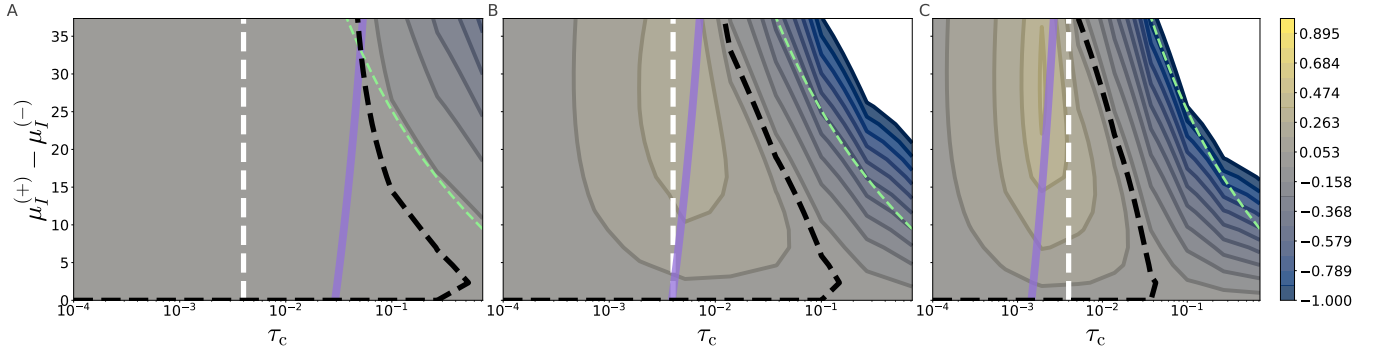


FIG. 25. Contour plot of the excess of SNR with respect to the absence of noise correlations, as in Fig. 10, except that panels A,B,C correspond, respectively, to different values of $\alpha_V = 0.25, 0.9, 1.5$. The rest of the model parameters are: $\mu_I^{(-)} = 45$, $\tau_m = 0.04$, $\sigma_V = 1.104$, $\alpha_V = 0.9$, $w = 0.45$.

-
- [1] E. Vaadia, I. Haalman, M. Abeles, H. Bergman, Y. Prut, H. Slovin, and A. Aertsen, Dynamics of neuronal interactions in monkey cortex in relation to behavioural events, *Nature* **373**, 515 (1995).
 - [2] M. A. Wilson and B. L. McNaughton, Dynamics of the hippocampal ensemble code for space, *Science* **261**, 1055 (1993).
 - [3] C. Gray, P. König, A. Engel, and W. Singer, Oscillatory responses in cat visual cortex exhibit inter-columnar synchronization which reflects global stimulus properties, *Nature* **338**, 334 (1989).
 - [4] D. N. Mastronarde, Correlated firing of cat retinal ganglion cells. ii. responses of x- and y-cells to single quantal events, *Journal of Neurophysiology* **49**, 325 (1983).
 - [5] A. E. Urai, B. Doiron, A. M. Leifer, and A. K. Churchland, Large-scale neural recordings call for new insights to link brain and behavior, *Nature Neuroscience* **25**, 11 (2022).
 - [6] C. Stringer and M. Pachitariu, Analysis methods for large-scale neuronal recordings, *Science* **375**, 1234 (2024).
 - [7] B. B. Averbeck, P. E. Latham, and A. Pouget, Neural correlations, population coding and computation, *Nature reviews neuroscience* **7**, 358 (2006).
 - [8] S. Panzeri, M. Moroni, H. Safaai, and C. D. Harvey, The structures and functions of correlations in neural population codes, *Nature Reviews Neuroscience* **23**, 551 (2022).
 - [9] A. T. Kuan, G. Bondanelli, L. N. Driscoll, J. Han, M. Kim, D. G. C. Hildebrand, B. J. Graham, D. E. Wilson, L. A. Thomas, S. Panzeri, C. D. Harvey, and W.-C. A. Lee, Synaptic wiring motifs in posterior parietal cortex support decision-making, *Nature* **627**, 367 (2024).
 - [10] N. Brunel and S. Sergi, Firing frequency of leaky integrate-and-fire neurons with synaptic current dynamics, *Journal of Theoretical Biology* **195**, 87 (1998).
 - [11] R. Kempter, W. Gerstner, J. L. Van Hemmen, and H. Wagner, Extracting oscillations: Neuronal coincidence detection with noisy periodic spike input, *Neural computation* **10**, 1987 (1998).
 - [12] J. Feng and D. Brown, Impact of Correlated Inputs on the Output of the Integrate-and-Fire Model, *Neural Computation* **12**, 671 (2000), <https://direct.mit.edu/neco/article-pdf/12/3/671/814408/089976600300015745.pdf>.
 - [13] N. Brunel, F. S. Chance, N. Fourcaud, and L. F. Abbott, Effects of synaptic noise and filtering on the frequency response of spiking neurons, *Physical Review Letters* **86**, 2186 (2001).
 - [14] E. Salinas and T. J. Sejnowski, Impact of correlated synaptic input on output firing rate and variability in simple neuronal models, *Journal of Neuroscience* **20**, 6193 (2000), <https://www.jneurosci.org/content/20/16/6193.full.pdf>.
 - [15] E. Salinas and T. J. Sejnowski, Integrate-and-fire neurons driven by correlated stochastic input, *Neural Computation* **14**, 2111 (2002).
 - [16] N. Fourcaud and N. Brunel, Dynamics of the firing probability of noisy integrate-and-fire neurons, *Neural Computation* **14**, 2057 (2002).
 - [17] R. Moreno, J. de la Rocha, A. Renart, and N. Parga, Response of spiking neurons to correlated inputs, *Phys. Rev. Lett.* **89**, 288101 (2002).
 - [18] J. Middleton, M. J. Chacron, B. Lindner, and A. Longtin, Firing statistics of a neuron model driven by long-range correlated noise, *Physical Review E* **68**, 021920 (2003).
 - [19] R. Moreno-Bote and N. Parga, Role of synaptic filtering on the firing response of simple model neurons, *Phys. Rev. Lett.* **92**, 028102 (2004).
 - [20] B. Lindner, Interspike interval statistics of neurons driven by colored noise, *Phys. Rev. E* **69**, 022901 (2004).
 - [21] T. Schwalger and L. Schimansky-Geier, Interspike interval statistics of a leaky integrate-and-fire neuron driven by gaussian noise with large correlation times, *Phys. Rev. E* **77**, 031914 (2008).
 - [22] B. Lindner, Some unsolved problems relating to noise in biological systems, *Journal of Statistical Mechanics: Theory and Experiment* **2009**, P01008 (2009).

- [23] A. Kohn, R. Coen-Cagli, I. Kanitscheider, and A. Pouget, Correlations and neuronal population information, *Annual Review of Neuroscience* **39**, 237 (2016).
- [24] E. Salinas and T. J. Sejnowski, Correlated neuronal activity and the flow of neural information, *Nature reviews neuroscience* **2**, 539 (2001).
- [25] L. F. Abbott and P. Dayan, The Effect of Correlated Variability on the Accuracy of a Population Code, *Neural Computation* **11**, 91 (1999), <https://direct.mit.edu/neco/article-pdf/11/1/91/814066/089976699300016827.pdf>.
- [26] E. Zohary, M. N. Shadlen, and W. T. Newsome, Correlated neuronal discharge rate and its implications for psychophysical performance, *Nature* **370**, 140 (1994).
- [27] S. Panzeri, S. R. Schultz, A. Treves, and E. T. Rolls, Correlations and the encoding of information in the nervous system, *Proceedings of the Royal Society of London. Series B: Biological Sciences* **266**, 1001 (1999).
- [28] S. Panzeri and S. R. Schultz, A Unified Approach to the Study of Temporal, Correlational, and Rate Coding, *Neural Computation* **13**, 1311 (2001), <https://direct.mit.edu/neco/article-pdf/13/6/1311/814847/08997660152002870.pdf>.
- [29] R. Moreno-Bote, J. Beck, I. Kanitscheider, X. Pitkow, P. Latham, and A. Pouget, Information-limiting correlations, *Nature neuroscience* **17**, 1410 (2014).
- [30] O. I. Rumyantsev, J. A. Lecoq, O. Hernandez, Y. Zhang, J. Savall, R. Chrapkiewicz, J. Li, H. Zeng, S. Ganguli, and M. J. Schnitzer, Fundamental bounds on the fidelity of sensory cortical coding, *Nature* **580**, 100 (2020).
- [31] R. Bartolo, R. C. Saunders, A. R. Mitz, and B. B. Averbeck, Information-limiting correlations in large neural populations, *Journal of Neuroscience* **40**, 1668 (2020).
- [32] M. Valente, G. Pica, G. Bondanelli, M. Moroni, C. A. Runyan, A. S. Morcos, C. D. Harvey, and S. Panzeri, Correlations enhance the behavioral readout of neural population activity in association cortex, *Nature neuroscience* **24**, 975 (2021).
- [33] J. I. Gold and M. N. Shadlen, Neural computations that underlie decisions about sensory stimuli, *Trends in cognitive sciences* **5**, 10 (2001).
- [34] C. A. Runyan, E. Piasini, S. Panzeri, and C. D. Harvey, Distinct timescales of population coding across cortex, *Nature* **548**, 92 (2017).
- [35] N. A. Francis, S. Mukherjee, L. Koçillari, S. Panzeri, B. Babadi, and P. O. Kanold, Sequential transmission of task-relevant information in cortical neuronal networks, *Cell Reports* **39**, 110878 (2022).
- [36] H. Safaai, A. Y. Wang, S. Kira, S. B. Malerba, S. Panzeri, and C. D. Harvey, Specialized structure of neural population codes in parietal cortex outputs, *bioRxiv* 10.1101/2023.08.24.554635 (2023).
- [37] E. Balaguer-Ballester, R. Nogueira, J. M. Abofalia, R. Moreno-Bote, and M. V. Sanchez-Vives, Representation of foreseeable choice outcomes in orbitofrontal cortex triplet-wise interactions, *PLoS Computational Biology* **16**, e1007862 (2020).
- [38] N. Shahidi, A. R. Andrei, M. Hu, and V. Dragoi, High-order coordination of cortical spiking activity modulates perceptual accuracy, *Nature Neuroscience* **22**, 1148 (2019).
- [39] J. Zylberberg, A. Pouget, P. E. Latham, and E. Shea-Brown, Robust information propagation through noisy neural circuits, *PLOS Computational Biology* **13**, 1 (2017).
- [40] C. Koch, M. Rapp, and I. Segev, A brief history of time (constants), *Cerebral cortex* **6**, 93 (1996).
- [41] V. Koren, G. Bondanelli, and S. Panzeri, Computational methods to study information processing in neural circuits, *Computational and Structural Biotechnology Journal* **21**, 910 (2023).
- [42] A. N. Burkitt, A review of the integrate-and-fire neuron model: I. homogeneous synaptic input, *Biological cybernetics* **95**, 1 (2006).
- [43] H. Risken and H. Risken, *Fokker-planck equation* (Springer, 1996).
- [44] R. Livi and P. Politi, *Nonequilibrium Statistical Physics: A Modern Perspective* (Cambridge University Press, 2017).
- [45] A. N. Burkitt, A review of the integrate-and-fire neuron model: Ii. inhomogeneous synaptic input and network properties, *Biological cybernetics* **95**, 97 (2006).
- [46] A. J. F. Siegert, On the first passage time probability problem, *Phys. Rev.* **81**, 617 (1951).
- [47] D. J. Amit and V. Martin-Mayor, *Field theory, the renormalization group, and critical phenomena* (McGraw-Hill International Book Co., 2005).
- [48] M. Ibanez-Berganza, *Coincidence-detection* code repository, <https://github.com/berganzami/coincidence-detection> (2024).
- [49] B. Walter, G. Pruessner, and G. Salbreux, First passage time distribution of active thermal particles in potentials, *Phys. Rev. Res.* **3**, 013075 (2021).
- [50] V. Buendía, P. Villegas, S. Di Santo, A. Vezzani, R. Burioni, and M. A. Muñoz, Jensen’s force and the statistical mechanics of cortical asynchronous states, *Scientific reports* **9**, 15183 (2019).
- [51] The recent results [49, 53] manage to have an approximated expression for the first-passage time distribution of an active Brownian particle (a non-Markovian random walker) for small $\nu_W = \sigma_c^2 \tau_m / (\sigma_I^2 \tau_c)$.
- [52] Notice that both the Moreno solution and the quenched-noise solution exhibit a constant behaviour in τ_c for large τ_c (and constant v_c), as expected from Eqs. (9,10).
- [53] B. Walter, G. Pruessner, and G. Salbreux, Field theory of survival probabilities, extreme values, first-passage times, and mean span of non-markovian stochastic processes, *Phys. Rev. Res.* **4**, 043197 (2022).
- [54] G. Ariav, A. Polsky, and J. Schiller, Submillisecond precision of the input-output transformation function mediated by fast sodium dendritic spikes in basal dendrites of ca1 pyramidal neurons, *Journal of Neuroscience* **23**, 7750 (2003).
- [55] M. London and M. Häusser, Dendritic computation, *Annual Review of Neuroscience* **28**, 503 (2005).
- [56] G. W. A. Constable, A. J. McKane, and T. Rogers, Stochastic dynamics on slow manifolds, *Journal of Physics A: Mathematical and Theoretical* **46**, 295002 (2013).
- [57] G. A. Pavliotis, *Stochastic processes and applications*, *Texts in applied mathematics* **60** (2014).
- [58] C. Bucher and M. Di Paola, Efficient solution of the first passage problem by path integration for normal and poissonian

- white noise, *Probabilistic Engineering Mechanics* **41**, 121 (2015).
- [59] C. C. Chow and M. A. Buice, Path integral methods for stochastic differential equations, *The Journal of Mathematical Neuroscience (JMN)* **5**, 1 (2015).
 - [60] R. Mannella, Integration of stochastic differential equations on a computer, *International Journal of Modern Physics C* **13**, 1177 (2002).
 - [61] P. E. Kloeden and E. Platen, *Numerical Solution of Stochastic Differential Equations*, Vol. 23 (Springer Science & Business Media, 2011).
 - [62] M. Newville, R. Otten, A. Nelson, T. Stensitzki, A. Ingargiola, D. Allan, A. Fox, F. Carter, Micha, R. Osborn, D. Pustakhod, S. Weigand, Ineuhaus, A. Aristov, Glenn, Mark, mgunyho, C. Deil, A. L. R. Hansen, G. Pasquevich, L. Foks, N. Zobrist, O. Frost, Stuermer, J.-C. Jaskula, S. Caldwell, P. Eendebak, M. Pompili, J. H. Nielsen, and A. Persaud, *lmfit/lmfit-py*: 1.3.2 (2024).
 - [63] T. M. Cover, *Elements of information theory* (John Wiley & Sons, 1999).

TABLE II. Symbols used in the article.

symbol	definition	description
$\mathbf{x}^{(s)}(t)$	$\dot{\mathbf{x}}(t) = (\boldsymbol{\mu}^{(s)} - \mathbf{x}(t))/\tau_c + (2C/\tau_c)^{1/2} \cdot \boldsymbol{\eta}(t)$	vector of instantaneous firing rates of encoding neurons
$\langle \cdot \rangle_{\boldsymbol{\eta}}$		average with respect to the distribution of white noises
$\boldsymbol{\mu}^{(s)}$	$= \langle \mathbf{x}^{(s)}(t) \rangle_{\boldsymbol{\eta}}$	vector of encoding average firing rates (tuning curves)
$\Delta \boldsymbol{\mu}$	$\boldsymbol{\mu}^{(+)} - \boldsymbol{\mu}^{(s-)}$	
C_{ij}	$= \text{Cov}(x_i(t), x_j(t))$	covariance matrix (element) between encoding rates
τ_c	$\text{Cov}(x_i(t), x_j(t')) = C_{ij} e^{- t-t' /\tau_c}$	noise correlation time
v_{V_i}	$= C_{ii}$	stationary variance of single encoding neurons
σ_{V_i}	$v_{V_i} = \sigma_{V_i}^2 / \tau_c$	count standard deviation of single encoding neurons
\bar{C}_{ij}	$= C_{ij} / (C_{ii} C_{jj})^{1/2}$	noise correlation matrix (element)
α_V	$\bar{C}_{ij} = \delta_{ij} + (1 - \delta_{ij}) \alpha_V$	Valente angle
$t_k^{(i)}$		k -th spike of the i -th encoding neuron
$\rho_i(t)$	$= \sum_{k>0} \delta(t - t_k^{(i)})$	density of spikes of encoding neuron i (single realisation)
$\rho(t)$	$= \sum_j \rho_j(t)$	density of encoding spikes in a single realisation
$n(T_c)$	$\int_0^{T_c} dt \rho(t)$	number of encoding spikes in a single realisation
$V(t)$		membrane potential of the readout LIF neuron
τ_m		membrane potential timescale of the readout LIF neuron
$I(t)$	$\dot{V}(t) = -V(t)/\tau_m + I(t)$	input current (the s -dependence is often omitted)
\mathbf{w}	$I(t) = \mathbf{w} \cdot \boldsymbol{\rho}(t)$	vector of gains
σ_I	$I(t) = \mu_I + \sigma_I \eta(t) + \sigma_c \xi(t)$	white-noise amplitude of the afferent current (diffusion app.)
σ_c		colored-noise (count) amplitude of the afferent current (diffusion app.)
v_c	$= \sigma_c^2 / (2\tau_c)$	colored-noise stationary variance of the afferent current (diffusion app.)
μ_I	$= \langle I(t) \rangle_{\eta, \xi}$	average input current (diffusion app.)
$\eta(t), \xi(t)$		white and colored noises (diffusion app.)
t_k		k -th spike of the readout neuron
$\varrho(t)$	$= \sum_{k>0} \delta(t - t_k)$	density of spikes (firing rate) of the readout neuron (single realization)
r_R	$= \langle \varrho(t) \rangle_{\eta, \xi}$	mean of the LIF readout neuron firing rate (or mean of a colored-noise LIF neuron firing rate)
v_R	$= \text{Var}_{\eta, \xi}(\varrho(t))$	variance of the readout neuron firing rate (or variance of a colored-noise LIF neuron firing rate)
T_c		length of the time chunk (in which the readout spikes are registered)
$n_R(T_c)$	$\int_0^{T_c} dt \varrho(t)$	number of readout spikes in a single realisation
r_w		Siebert solution for the mean rate of a white-noise LIF neuron
t_w	$= r_w^{-1}$	Siebert solution for the mean ISI of a white-noise LIF neuron
α_M	$= \sigma_c^2 / \sigma_I^2$	Moreno parameter
r_q		quenched-noise approximation for r_R
v_q		quenched-noise approximation for v_R
r_M		Moreno et al approximation for r_R
g_1	$= r_w' / r_w$	
μ_I^*		inflection point of r_w
readout rate	$= n_R(T_c) / T_c$	number of readout spikes per unit time in a window of length T_c (or number of spikes per unit time of a general LIF neuron)
$C(t)$	$= \langle \varrho(t') \varrho(t' + t) \rangle_{\xi, \eta} - r_R^2$	temporal correlation function of the readout neuron
$C_-(t)$	$C(t) = a \delta(t) + C_-(t)$	regular part of C
$g(t)$	$C(t) = r_R g(t) - r_R^2$	readout neuron temporal distribution function
Δr_R	$= r_R^{(+)} - r_R^{(-)}$	
μ_I^*		inflection point of r_w
$\hat{\mu}_I$		upper bound of $\mu_I^{(+)}$ for the SNR to increase (see IV B)
$\hat{\mu}_I^{(-)}$		lower bound of $\mu_I^{(-)}$ for the SNR to increase (see IV B)
n_{is}		number of integration steps per unit time (see C)

TABLE III. Parameters of the first simulation set.

variable	varying	value/range
τ_c	yes	10^{-4+a} , $a = (0, b, 2b, \dots, 9b)$ with $b = 3/7$ =1.000e-4, 2.682e-4, 7.196e-4, 1.930e-3, 5.179e-3, 1.389e-2, 3.727e-2, 1.000e-1, 2.682e-1, 7.196e-1
n_{is}	yes	2^m , with $m = (13, \dots, 18)$ = 8192, 16384, 32768, 65536, 131072
μ_I	yes	$32 + m\delta_{\mu_I}$, with $m = (0, \dots, 8)$ and $\delta\mu_I = 2.95$ =32.65, 35.6, 38.55, 41.5, 44.45, 47.4, 50.35, 53.3, 56.25
α_V	yes	0.0, 0.9
τ_m	no	0.005
v_V	no	9.795
w	no	0.45
n_{tr}	no	1000

TABLE IV. Parameters of the second simulation set.

variable	varying	value/range
μ_I	yes	$32 + m\delta_{\mu_I}$, with $m = (0, \dots, 8)$ and $\delta\mu_I = 2.95$ =32.65, 35.6, 38.55, 41.5, 44.45, 47.4, 50.35, 53.3, 56.25
α_V	yes	0.0, 0.9
τ_c	no	0.1
n_{is}	no	131072
τ_m	no	0.005
v_V	no	25.39
w	no	0.45
n_{tr}	no	1000

TABLE V. Two-time correlator of the input current, $c(|t - t'|) := \langle (I(t) - \mu_I)(I(t') - \mu_I) \rangle$ in the two different scenarios: constant instantaneous colored noise amplitude σ_c (and τ_c -dependent stationary noise amplitude v_c); constant v_c (and τ_c -dependent σ_c) (from equation (7)).

	$\tau_c = 0$	$\tau_c = \infty$
constant $v_c = \sigma_c^2 / (2\tau_c)$	$c(t - t') = \sigma_I^2 \delta(t - t')$	$c(t - t') = \sigma_I^2 \delta(t - t') + v_c$
constant σ_c	$c(t - t') = (\sigma_I^2 + \sigma_c^2) \delta(t - t')$	$c(t - t') = \sigma_I^2 \delta(t - t')$